Collective excitations of ^{96}Ru by means of $(p, p'\gamma)$ experiments

A. Hennig,[1,*] T. Ahn,[2,†] V. Anagnostatou,[2,3] A. Blazhev,[1] N. Cooper,[2] V. Derya,[1] M. Elvers,[1,2] J. Endres,[1] P. Goddard,[2,3] A. Heinz,[2,4] R. O. Hughes,[2,5] G. Ilie,[2,6] M. N. Mineva,[7,8] P. Petkov,[1,6,7] S. G. Pickstone,[1] N. Pietralla,[9,10] D. Radeck,[1,2] T. J. Ross,[3,5] D. Savran,[11,12] M. Spieker,[1] V. Werner,[2,9] and A. Zilges[1]

[1]*Institut für Kernphysik, Universität zu Köln, D-50937 Köln, Germany*
[2]*Wright Nuclear Structure Laboratory, Yale University, New Haven, Connecticut 06520, USA*
[3]*Department of Physics, University of Surrey, Guildford, GU2 7XH, United Kingdom*
[4]*Fundamental Fysik, Chalmers Tekniska Högskola, SE-41296 Göteborg, Sweden*
[5]*University of Richmond, Richmond, Virginia 23173, USA*
[6]*National Institute for Physics and Nuclear Engineering, RO-77125 Bucharest-Magurele, Romania*
[7]*Institute for Nuclear Research and Nuclear Energy, Bulgarian Academy of Sciences, BG-1784 Sofia, Bulgaria*
[8]*Faculty of Physics, University of Sofia, BG-1164 Sofia, Bulgaria*
[9]*Institut für Kernphysik, Technische Universität Darmstadt, D-64289 Darmstadt, Germany*
[10]*GSI Helmholtzzentrum, D-64291, Darmstadt, Germany*
[11]*ExtreMe Matter Institute EMMI and Research Division, GSI, D-64291 Darmstadt, Germany*
[12]*Frankfurt Institute for Advanced Studies FIAS, D-60438 Frankfurt am Main, Germany*

(Received 28 October 2015; published 21 December 2015)

Background: One-phonon mixed-symmetry quadrupole excitations are a well-known feature of near-spherical, vibrational nuclei. Their interpretation as a fundamental building block of vibrational structures is supported by the identification of multiphonon states resulting from a coupling of fully-symmetric and mixed-symmetric quadrupole phonons. In addition, the observation of strong $M1$ transitions between low-lying 3^- and 4^+ states has been interpreted as an evidence for one-phonon mixed-symmetry excitations of octupole and hexadecapole character.

Purpose: The aim of the present study is to identify collective one- and two-phonon excitations in the heaviest stable $N = 52$ isotone ^{96}Ru based on a measurement of absolute $M1$, $E1$, and $E2$ transition strengths.

Methods: Inelastic proton-scattering experiments have been performed at the Wright Nuclear Structure Laboratory (WNSL), Yale University, and the Institute for Nuclear Physics (IKP), University of Cologne. From the acquired proton-γ and $\gamma\gamma$ coincidence data we deduced spins of excited states, γ-decay branching ratios, and multipole mixing ratios, as well as lifetimes of excited states via the Doppler-shift attenuation method (DSAM).

Results: Based on the new experimental data on absolute transition strengths, we identified the 2^+ and 3^+ members of the two-phonon mixed-symmetry quintuplet $(2^+_{1,\mathrm{ms}} \otimes 2^+_{1,\mathrm{s}})$. Furthermore, we observed strong $M1$ transitions between low-lying 3^- and 4^+ states suggesting one-phonon symmetric and mixed-symmetric octupole and hexadecapole components in their wave functions, respectively. The experimental results are compared to sdg-IBM-2 and shell-model calculations.

Conclusions: Both the sdg-IBM-2 and the shell-model calculations are able to describe key features of mixed-symmetry excitations of ^{96}Ru. Moreover, they support the one-phonon mixed-symmetry hexadecapole assignment of the experimental 4^+_2 state.

DOI: 10.1103/PhysRevC.92.064317 PACS number(s): 21.10.Re, 21.10.Tg, 23.20.Lv, 21.60.Ev

I. INTRODUCTION

Protons and neutrons are the building blocks of atomic nuclei. Because of the two-component character, the isospin degree of freedom has to be considered for their description. This features excitation modes that are symmetric or antisymmetric under pairwise exchange of protons and neutrons and are denoted as fully-symmetric and mixed-symmetric states, respectively [1–3]. Mixed-symmetry states are naturally predicted in the framework of the sd proton-neutron version of the interacting boson model (sd-IBM-2) [4–7]. The model accounts for the pairing force by coupling like valence nucleons to pairs with $L = 0$ and $L = 2$, treated as bosons, i.e., s and d bosons. In the IBM-2, the proton-neutron symmetry of the wave functions of excited states can be obtained from the F-spin quantum number [5,6], which is the bosonic analog of isospin for fermions: states with maximum F-spin quantum number $F = F_{\max}$ are unchanged under pairwise exchange of proton and neutron bosons and are therefore referred to as fully-symmetric states, while states with nonmaximum F-spin quantum number are denoted as mixed-symmetry states. Besides the description in the IBM-2 framework, the properties of mixed-symmetry states have successfully been obtained from shell-model and quasiparticle-phonon model (QPM) calculations; see, e.g., Refs. [8,9].

Experimentally, mixed-symmetry quadrupole states can be identified by their specific $E2$ and $M1$ decay

*hennig@ikp.uni-koeln.de
†Present address: Department of Physics, University of Notre Dame, Notre Dame, Indiana 46556, USA.

properties [10]:

(i) Strong $M1$ transitions with matrix elements in the order of 1 μ_N^2 to their symmetric counterparts.
(ii) Weakly collective $E2$ transitions to symmetric states reducing the phonon number by 1. The corresponding $B(E2)$ values are in the order of a few W.u. or less.
(iii) Collective $E2$ transitions among mixed-symmetry states with $B(E2)$ values comparable to that of the $2_1^+ \rightarrow 0_1^+$ transition.

Based on these experimental signatures, extensive studies of mixed-symmetry states have been performed in the $A \approx 100$ mass region and, in particular, on the nucleus ^{94}Mo [11–14], which is up to now the prime example for low-lying mixed-symmetry structures. Moreover, states with mixed-symmetry character are also found in the other stable $N = 52$ nuclei ^{92}Zr [15,16], ^{93}Nb [17], and ^{96}Ru [18–20], as well as in the vicinity of the $Z = 28,50$ and $N = 28,82$ shell closures; see, e.g., Refs. [10,21] for a review.

The interpretation of the mixed-symmetry quadrupole phonon as a fundamental building block of vibrational structures in atomic nuclei becomes particularly evident in the Q-phonon scheme [22–24], which provides an intuitive and semiquantitative picture of mixed-symmetry states. In this formalism, the lowest-lying symmetric and mixed-symmetric states, labeled in the following as $2^+_{1,\mathrm{s}}$ and $2^+_{1,\mathrm{ms}}$, respectively, can be described in terms of Q-phonon excitations of the correlated ground state. In particular, the combination of a symmetric and a mixed-symmetry Q-phonon excitation results in a quintuplet of mixed-symmetry states with spin and parity quantum numbers $J = 0^+, 1^+, 2^+, 3^+$, and 4^+ [1,12,13].

In addition to the quadrupole case, mixed-symmetry states of octupole and hexadecapole character have been proposed recently [25,26]. The assignment is based on the experimental observation of strong $M1$ transitions with $B(M1)$ values in the order of 1 μ_N^2 connecting low-lying 3^- and 4^+ states, respectively. Candidates for mixed-symmetry octupole excitations have been proposed for several vibrational nuclei in the $A \approx 100$ mass region, among others also for the $N = 52$ isotones ^{92}Zr and ^{94}Mo. This excitation mode was predicted in sdf-IBM-2 calculations [27], suggesting strong $E1$ transitions to the symmetric one-phonon quadrupole excitation as an additional signature along with the $M1$ fingerprint. First evidences for enhanced F-vector $E1$ transitions have been observed indeed in a few selected cases [28].

Similarly, one-phonon mixed-symmetry hexadecapole excitations were described by taking into account the hexadecapole degree of freedom in IBM-2 calculations, i.e., in the scope of sdg-IBM-2 calculations for ^{94}Mo [26]. In a recent paper, we adopted this approach for the description of the exceptionally large $M1$ strength of the $4_2^+ \rightarrow 4_1^+$ transition in ^{96}Ru [29]. It is the purpose of this paper to provide more comprehensive information on the recently performed experiments on ^{96}Ru and their results, focusing on the identification of the 2^+ and 3^+ members of the two-phonon mixed-symmetry quintuplet as well as on symmetric quadrupole-octupole coupled states. Moreover, we present shell-model calculations aiming for the description of the strong $4_2^+ \rightarrow 4_1^+$ $M1$ transition in ^{96}Ru within a microscopic model and to compare the results with those from an algebraic approach in the sdg-IBM-2 framework.

Section II describes the experimental details, while the results and their discussion are presented in Secs. III and IV. Results of the sdg-IBM-2 calculations are shown in Sec. V, focusing on two-phonon mixed-symmetry states that have not been discussed in our previous article [29]. The shell-model calculations and a comparison of the experimental data to the neighboring $N = 52$ nuclei ^{92}Zr and ^{94}Mo are presented in Secs. VI and VII, respectively.

II. EXPERIMENTAL DETAILS

Two inelastic proton-scattering experiments were performed to extract comprehensive spectroscopic information on excited low-spin states of ^{96}Ru. The experiment at the Wright Nuclear Structure Laboratory (WNSL), Yale University, USA, was performed to extract spins of excited states as well as branching ratios and multipole mixing ratios of deexciting γ-ray transitions. To extract nuclear level lifetimes an additional proton-scattering experiment was performed at the Institute for Nuclear Physics (IKP), University of Cologne, Germany. Both experiments are described in the following.

A. The ^{96}Ru$(p,p'\gamma)$ experiment at WNSL, Yale

An 8.4 MeV proton beam, provided by the ESTU Tandem accelerator impinged on a 106 μg/cm^2 isotopically enriched ^{96}Ru target supported by a ^{12}C backing with a thickness of 14 μg/cm^2. Data were acquired for 134 hours at an average beam current of 50 nA.

Deexciting γ rays were detected with eight bismuth germanate (BGO)-shielded Clover-type high-purity germanium (HPGe) detectors of the YRAST ball spectrometer [30] positioned at 45° (2×), 90° (5×), and 135° (1×) with respect to the beam axis. The energy of the scattered protons was measured with five silicon detectors mounted inside the target chamber at angles of 135°, 133°, 131°, 119°, and 90° with respect to the beam axis. In an off-beam calibration, an energy resolution of 70 keV was obtained for the particle detectors. Because of the energy straggling of the protons in the target material and kinematic effects, the energy resolution degraded to 146 keV for the in-beam particle spectra. For the data acquisition, four triggers were implemented, namely $p\gamma$ and $\gamma\gamma$ coincidences as well as downscaled single-γ and single-proton events. Further details of the experimental setup can be found in Ref. [31]. The list-mode data were processed using the sorting code CSCAN. Randomly coincident events were eliminated by subtracting peak and background matrices that were obtained by gating on the prompt peak and random background events in the acquired time-difference spectra. An excerpt of the acquired proton-γ coincidence matrix is shown in Fig. 1(a). Transitions appear as thin horizontal lines due to the worse energy resolution in the particle spectra compared to the γ-ray spectra.

From the energies of the scattered protons the excitation energies E_x of the residual ^{96}Ru nuclei were extracted. By applying gating conditions on the excitation energy of a

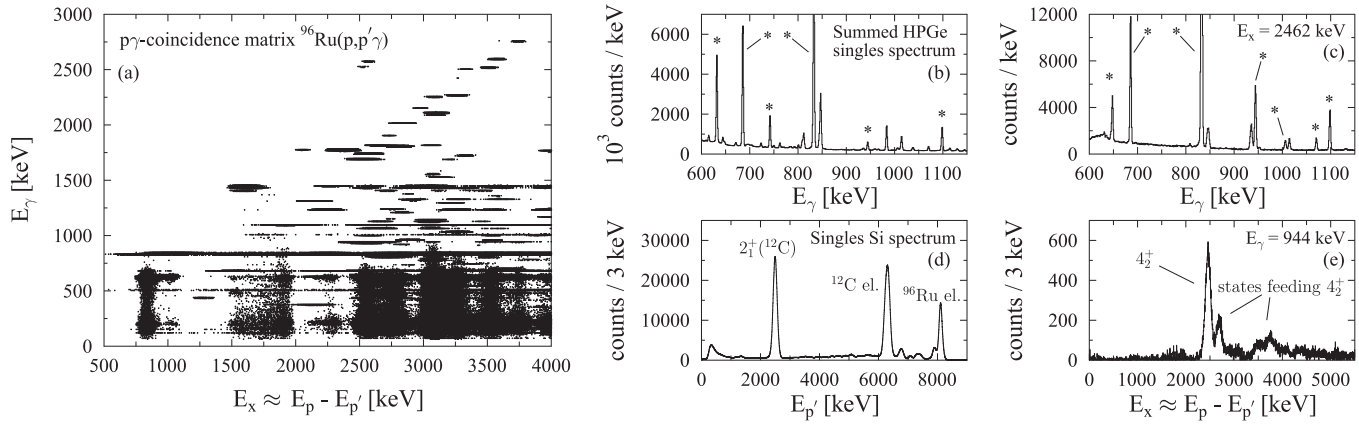

FIG. 1. (a) Proton-γ coincidence matrix obtained in the ^{96}Ru experiment at WNSL, Yale. Transitions stemming from ^{96}Ru are visible as thin horizontal lines due to the better energy resolution of the HPGe detectors compared to the silicon particle detectors. (b) The summed HPGe singles spectrum is already dominated by transitions of ^{96}Ru, marked with asterisks. (c) By applying a proton gate on the excitation energy of the 4_2^+ state of ^{96}Ru at $E_x = 2462$ keV, the peak-to-background ratio is significantly improved. (d) The proton singles spectrum is dominated by elastically scattered protons and reactions in the backing material. (e) Applying a γ gate on the $4_2^+ \rightarrow 4_1^+$ transition at $E_\gamma = 944$ keV reveals peaks in the excitation spectrum corresponding to the excitation of the 4_2^+ level as well as states feeding the 4_2^+ state.

particular excited state γ-ray spectra were generated that contain its deexciting transitions as well as their subsequent γ decays. This allows us to easily construct the level scheme of ^{96}Ru. The additionally acquired $\gamma\gamma$ coincidence data were used to resolve remaining ambiguities. Furthermore, γ-decay branching ratios were extracted with high sensitivity because of the increased peak-to-background ratio compared to, e.g., the γ-ray singles spectra and, thus, even weak transitions could be resolved from the background. However, the γ-ray intensity detected in the HPGe detectors depends on the angular distribution of the emitted γ rays and thus on their multipolarity. Since for several transitions the multipole mixing ratio of the transitions, and in some cases even the spins of the involved states, are not known, a systematic error of 10% was assigned in addition to the statistical error for the γ-decay branching ratios.

From the $\gamma\gamma$ coincidence data acquired in the experiment spin quantum numbers J of excited states as well as multipole mixing ratios δ of γ ray transitions were extracted by means of the $\gamma\gamma$ angular correlation analysis, described in detail in, e.g., Ref. [32]. The $\gamma\gamma$ coincidence data were sorted into twelve groups that are characterized by the angles θ_1, θ_2, and Φ. θ_1 and θ_2 denote the angles of the two active HPGe detectors with respect to the beam axis and Φ is the angle between the planes spanned by the beam axis and the directions of γ-ray emission. For a cascade of two coincident γ rays with energies E_{γ_1} and E_{γ_2} and respective multipole mixing ratios δ_1 and δ_2 connecting successively states with spins J_1, J_2, and J_3, information on δ_1 and J_1 can be obtained by fitting the parameters of the angular correlation function $W(\theta_1,\theta_2,\Phi,J_1,J_2,J_3,\delta_1,\delta_2,\mu)$ to the efficiency-corrected coincidence intensity of the two γ rays. Here, μ denotes the width of the initial magnetic substate distribution and is treated as a free parameter. For the fits, the program RCORLEONE was used which explicitly takes the finite solid angles of the HPGe detectors into account. Sample fits to extract J_1 and δ_1 for several $\gamma\gamma$ cascades are shown in Fig. 2.

B. The ^{96}Ru$(p,p'\gamma)$ experiment at IKP, Cologne

To extract the lifetimes of excited states in the subpicosecond regime, the Doppler-shift attenuation method (DSAM) [33,34] is usually the method of choice. However, no lifetimes could be extracted from the experiment at WNSL since the energy-bin width of 1 keV in the γ-ray spectra acquired with the 4096 channel analog-to-digital converters (ADCs) did not allow for an extraction of Doppler shifts in

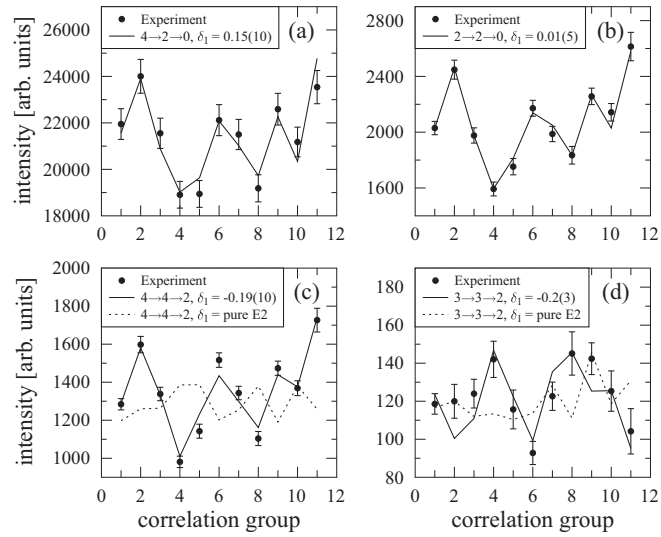

FIG. 2. Results of the $\gamma\gamma$ angular correlation analysis for the 1518 keV $\rightarrow$ 832 keV $\rightarrow$ g.s. (a), the 2283 keV $\rightarrow$ 832 keV $\rightarrow$ g.s. (b), the 2462 keV $\rightarrow$ 1518 keV $\rightarrow$ 832 keV (c), and the 3077 keV $\rightarrow$ 1818 keV $\rightarrow$ 832 keV (d) cascades. The obtained multipole mixing ratios δ_1 of the first transitions are quoted in the insets. A dominant $M1$ character is obtained for the 2462 keV $\rightarrow$ 1518 keV (c) and 3077 keV $\rightarrow$ 1818 keV (d) transitions. In contrast, an assumed pure $E2$ character cannot describe the experimental data for those transitions.

the sub-keV regime. Therefore, a second proton-scattering experiment was performed at the Institute for Nuclear Physics at the University of Cologne, Germany, aimed at lifetime measurements.

The same target used for the previous experiment was bombarded with a 7.0 MeV proton beam, provided by the 10 MV FN Tandem accelerator. γ rays were detected using the HORUS γ-ray spectrometer, equipped with 12 single-crystal and two Clover-type HPGe detectors positioned at angles of 35° (2×), 45° (2×), 90° (6×), 135° (2×), and 145° (2×) with respect to the beam axis. Four of the single-crystal and the two Clover-type detectors were equipped with BGO shields for an active Compton suppression. As in the experiment at WNSL, the scattered protons were detected in coincidence with the γ rays by six passivated implanted planar silicon (PIPS) detectors of the SONIC array [35]. The energy resolution of 15 keV achieved with calibration sources degraded to 70 keV in the in-beam proton spectra. The preamplifier signals of the detectors were processed with eight DGF-4C Rev. F modules [36], extracting the energy and time information of the signals by means of digital pulse processing techniques. The DGF-4C modules provide pulse-height spectra with 2^{15} channels which translates into a bin width of 0.12 keV. The small bin width as well as a careful energy calibration of the HPGe detectors were mandatory to extract centroid shifts in the sub-keV regime. To ensure the latter, a ^{56}Co source was mounted on the target ladder throughout the entire experiment, allowing for a run-by-run energy calibration. Data were acquired with a trigger on events with multiplicity two or higher. Randomly coincident events were eliminated in the same way as described in Sec. II A.

The centroid shift version of the Doppler-shift attenuation method utilizes the angular dependence of the energy centroid of the detected γ-ray peaks given by

$$E_\gamma(\Theta) = E_\gamma^0\left(1 + F(\tau)\frac{v_0}{c}\cos\Theta\right), \qquad (1)$$

where E_γ^0 is the energy of the unshifted γ ray, $F(\tau)$ the Doppler-shift attenuation factor, v_0 the initial recoil velocity, and Θ the angle between the initial direction of motion of the recoil nucleus and the direction of γ-ray emission [33]. As discussed in Refs. [37–39], the coincident detection of scattered protons and deexciting γ rays has several advantages. In particular, the lifetimes extracted from γ-ray spectra that were gated on the excitation energy of the level of interest are not affected by feeding contributions.

To extract an experimental value for the Doppler-shift attenuation factor $F(\tau)$, the $p\gamma$ coincidence data were sorted into eleven groups, characterized by different values of Θ. For several transitions, Fig. 3 shows the peak centroids obtained for each group as a function of the cos Θ value characterizing the group for several transitions. The value for $F(\tau)$ is obtained from a linear fit according to Eq. (1). Detailed information on the method of lifetime determination via the $(p, p'\gamma)$ reaction and the $p\gamma$-coincidence technique has been published in a dedicated article [39].

The slowing-down process of recoiling ^{96}Ru nuclei in the target (^{96}Ru) and stopper (^{12}C) materials was modeled by means of the Monte Carlo simulation code DSTOP96 [40] which is based on the code DESASTOP [41,42]. The electron stopping powers were obtained from the tables of Northcliffe and Schilling (NS) [43] and corrected for atomic electron structure effects following the approach of Ziegler and Chu [44,45]. The nuclear stopping was treated according to the theory of Lindhard, Scharff, and Schiøtt (LSS theory) [46] using a Thomas-Fermi screened Coulomb potential describing the interaction between the incident ion and the medium atoms in the form given in [47]. Finally, using the velocity profiles at different times during the deceleration as generated by the Monte Carlo simulation, theoretical values for the Doppler-shift attenuation factor $F(\tau)$ as a function of the lifetime were obtained to allow the derivation of the latter by comparison with the experimental value.

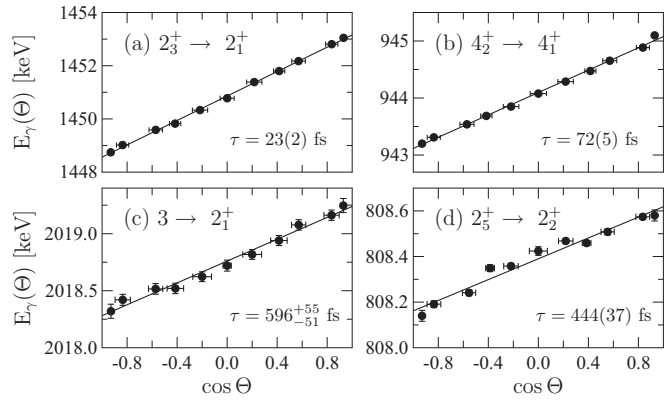

FIG. 3. Centroid shift of the γ-ray peaks obtained for the $2_3^+ \rightarrow 2_1^+$ transition (a), the $4_2^+ \rightarrow 4_1^+$ transition (b), the $3 \rightarrow 2_1^+$ transition with the $J = 3$ state at $E_x = 2851$ keV (c), and the $2_5^+ \rightarrow 2_2^+$ transition (d) as a function of cos Θ. The linear trend giving the Doppler-shift attenuation factor is evident.

For the simulation of the slowing-down process the compositions and thicknesses of the target and stopper materials have to be known precisely. This was achieved by analyzing the target by means of an additional Rutherford backscattering spectrometry (RBS) measurement at the RUBION Dynamitron tandem accelerator laboratory at the Ruhr Universität Bochum, Germany, performed in the scope of this work.

In total, lifetimes of 30 excited states were determined. For those states where a previously measured lifetime value was available in literature, our new value is in remarkably good agreement [39]. For several states it was possible to analyze more than one depopulating transition. This results in two or even three independent lifetime values that are consistent within the experimental uncertainties.

III. RESULTS

The combined data of both experiments provide comprehensive spectroscopic information on low-spin states of the nucleus ^{96}Ru. They are compiled in Table I. The experimental level scheme obtained in this work is found to be in good agreement with the results of previous experiments [18,19,48,49]. Moreover, 45 new transitions and 10 new excited states were added to the level scheme. In the following we briefly discuss

TABLE I. Levels in ^{96}Ru obtained from the experiments at WNSL and at IKP Cologne. Levels, transitions, lifetimes, and multipole mixing ratios marked with * were determined for the first time. The quoted lifetime values are obtained in this work unless specified differently. Newly assigned or revised spin and parity quantum numbers are labeled with †. Otherwise, they are adopted from NNDC data sheets [50]. For the excitation energies E_x and the γ-ray energies E_γ, a systematic error of 0.1 keV and the standard deviation are taken into account.

E_x (keV)	J_i^π	J_f^π	E_γ (keV)	I_γ (%)	$\delta(J_i^\pi \to J_f^\pi)$	$F(\tau)$	τ (fs)
832.5(1)	2^+	0^+	832.5(1)	100			$4.2(3) \times 10^3$ [a]
1518.2(2)	4^+	2^+	685.3(1)	100			$9.95(13) \times 10^3$ [a]
1930.9(2)	2^+	2^+	1098.4(1)	100	$-1.1(2)$	0.177(10)	395^{+47}_{-43}
2148.5(2)	0^+	2^+	1315.9(1)	100		0.112(8)	678^{+90}_{-87}
2149.2(2)	6^+	4^+	631.4(1)	100			
2283.3(2)	2^+	0^+	2283.3(1)	7.2(9)		0.74(3)	23(2)
		2^+	1450.9(1)	100(11)	0.01(5)	0.779(10)	
		2^+	352.3(1)*	0.36(10)			
2462.3(2)	$4^{+\dagger}$	2^+	1629.7(1)*	4.2(8)			72(5)
		4^+	944.1(1)	100(11)	$-0.19(10)^*$	0.516(12)	
2524.4(6)	$3^+,4^+$	2^+	1692.3(1)	100(15)			100^{+9*}_{-10}
		4^+	1005.4(1)	29(4)		0.434(17)	
		2^+	593.7(2)	0.8(4)			
2528.0(2)	$1^+,2^+$	0^+	2527.8(1)	26(3)		0.494(18)	79(8)*
		2^+	1695.6(1)	100(12)			
		2^+	597.1(2)*	1.4(3)			
2575.7(4)	(2^+)	0^+	2575.7(1)	77(11)		0.396(9)	119^{+7*}_{-8}
		2^+	1742.8(2)	100(17)	$-0.09(11)^*$		
		2^+	645.2(2)*	12(2)			
2578.5(5)	$1^+,2^+,3^+$	2^+	1745.6(2)	100(15)			
		2^+	648.0(2)	49(7)	2.0^{+6}_{-5} [b]		
2588.6(2)	5^-	4^+	1070.2(1)	100	$-0.01(4)$	0.017(8)	>4000[c]
2650.0(2)	$3^{(-)}$	2^+	1817.4(1)	100(12)	0.02(4)*	0.131(4)	544^{+45*}_{-41}
		4^+	1131.6(1)	33(4)			
		2^+	719.0(1)	2.5(5)			
		2^+	366.7(2)	7.7(10)			
2699.7(2)	$4^{+\dagger}$	2^+	1867.0(2)*	3.5(9)			
		4^+	1181.5(1)	7.4(16)			
		4	237.7(2)	100(11)			
		$3^+,4^+$	175(2)	–[d]			
		5^-	111(2)	–[d]			
2739.7(5)	2^+	0^+	2739.5(1)*	1.9(3)			444(37)*
		2^+	1906.8(1)	33(4)	3^{+4*}_{-1}	0.163(9)	
		2^+	808.4(1)	100(11)	$-0.01(9)^*$	0.142(9)	
		0^+	591.4(2)	0.9(3)			
		2^+	456.2(2)	5.2(7)	$-0.20(17)^*$		
		$1^+,2^+$	211.8(2)*	2.7(4)			
2760.1(2)	$4^+,5$	4^+	1241.8(1)	100		0.74(3)	27(5)*
2794.0(4)	5,6	4^+	1275.5(2)	46(11)			
		6^+	644.2(2)	100(19)			
2851.4(2)	$3^\dagger$	2^+	2018.8(1)	100(11)	0.04(5)*	0.120(5)	596^{+55*}_{-51}
		4^+	1333.3(1)	26(3)			
		2^+	920.4(1)	10.0(13)			
		2^+	568.2(2)	6.4(9)			
2891.0(2)	6^+	6^+	741.8(1)	100			<300[e]
2897.6(3)	3^+	2^+	2064.9(1)	27(3)		0.17(2)	432^{+48*}_{-46}
		4^+	1379.4(1)	38(5)			
		2^+	966.3(1)	100(11)	0.07(4)*	0.147(11)	
		2^+	614.3(2)	6.5(12)			
		4^+	435.8(2)	11.5(16)			
		(2^+)	322.1(2)*	2.4(6)			
2987.8(2)	$0^{+\dagger}$	2^+	2155.3(1)	100		0.494(77)	77(7)*
2996.1(2)	$3^+,4^+$	2^+	2163.4(1)	100(13)		0.28(2)	205^{+31*}_{-30}
		4^+	1478.1(1)	19(3)			
		$3^+,4^+$	471.6(2)	18(3)			

TABLE I. (*Continued.*)

E_x (keV)	J_i^π	J_f^π	E_γ (keV)	I_γ (%)	$\delta(J_i^\pi \rightarrow J_f^\pi)$	$F(\tau)$	τ (fs)
3055.0(2)*	$2^+,3,4^+$	2^+	2222.4(2)*	54(7)		0.30(3)	181^{+29*}_{-30}
		4^+	1536.9(2)*	100(12)			
		2^+	1124.1(1)*	74(9)			
3059.9(4)	$4^{+\dagger}$	2^+	2227.0(2)	12.5(18)			
		2^+	1128.9(1)	100(11)	−0.00(15)*		
		6^+	911.0(2)*	1.7(5)			
		2^+	776.2(1)*	25(3)	0.4(3)*		
		$3^{(-)}$	410.4(2)	7.5(11)			
3072.8(2)	$4^\dagger$	$3^{(-)}$	422.7(2)*	63(8)	0.00(7)*		
		5^-	484.3(2)	100(12)			
3075.8(5)	$3^{(-)}$	2^+	2243.3(1)	6.8(11)			$0.73(12) \times 10^{3*}$
		4^+	1556.9(2)	45(5)			
		2^+	1144.8(1)	100(11)		0.099(11)	
		2^+	792.3(1)*	26(3)			
		4	615.0(2)	4.2(10)			
		$3^{(-)}$	426.2(2)	34(4)	− 0.2(3)*		
		$4^+,5^+$	376.7(2)*	14.9(19)			
3089.7(2)	2^+	0^+	3089.8(2)	3.4(6)		0.695(17)	32(3)*
		2^+	2257.0(1)	100(11)	− 0.6(2)*		
		2^+	1158.8(2)*	4.8(8)			
3154.3(2)	$1^{(+)}$	0^+	3154.1(1)	100(12)		0.89(2)	9(2)
		2^+	2322.0(2)	4.6(8)			
		2^+	1223.4(2)	12.0(17)			
3166.5(2)	(5,6)	4^+	1648.3(1)	100			
3208.1(3)	2,6	2^+	2375.5(1)	100(13)		0.87(5)	11(4)*
		4^+	1690.2(1)	95(25)		0.78(4)	
		2^+	1277.0(1)*	47(7)		0.82(9)	
3231.8(2)	$(2^+)^\dagger$	0^+	3231.9(2)*	12.7(18)			39(5)*
		2^+	2399.3(2)*	13.5(19)			
		2^+	1300.8(1)	100(12)	0.1(2)*	0.39(2)	
3261.5(8)	2^+	0^+	3262.3(2)	45(6)			48(11)*
		2^+	2428.1(1)	100(12)	− 0.06(12)*	0.65(3)	
		2^+	1331.7(1)	87(15)			
3282.4(2)	1	0^+	3282.2(1)	100(12)		0.66(3)	37(6)
		2^+	2450.0(2)*	42(6)			
		0^+	1133.8(2)*	9.4(17)			
3291.5(5)	4^+	2^+	2458.6(1)	100(17)		0.43(7)	100(29)*
		4^+	1773.8(2)	38(8)			
		$3^+,4^+$	766.9(1)	43(8)			
3339.4(3)*	$2,3^{+\dagger}$	2^+	2506.6(1)*	100(12)		0.125(12)	549^{+82*}_{-81}
		$2^+,3$	488.2(2)*	10.0(16)			
		4	279.9(2)*	6.5(10)			
3377.8(9)	5^+	6^+	1227.9(2)	100(17)			
		4^+	1860.2(2)	24(7)			
3398.1(3)*	$2^+,3,4^+$	2^+	2565.3(1)*	87(13)		0.27(3)	204^{+39*}_{-40}
		4^+	1880.2(1)*	61(10)			
		2^+	1466.9(1)*	75(11)			
		$3^{(-)}$	748.2(1)*	100(14)			
		$4^+,5$	698.4(1)*	41(7)			
3443.2(2)*		2^+	2610.7(2)*	16(4)			147(39)*
		2^+	1512.3(1)*	100(14)			
		$1^+,2^+$	915.1(1)*	57(8)		0.34(5)	
		$1^{(+)}$	289.0(2)*	13(2)			
3448.5(2)	1	0^+	3448.4(2)	100			182(31)[f]
3458.5(7)*		2^+	2626.2(2)*	16(3)			41(6)*
		2^+	1937.2(1)*	100(18)		0.64(3)	
		2^+	1527.5(1)*	76(12)			

TABLE I. (*Continued.*)

E_x (keV)	J_i^π	J_f^π	E_γ (keV)	I_γ (%)	$\delta(J_i^\pi \to J_f^\pi)$	$F(\tau)$	τ (fs)
3479.4(2)	1	0^+	3479.3(1)	100(12)		0.61(3)	47(6)
		2^+	2647.0(2)*	14(2)			
3493.1(2)*		4^+	1974.9(2)*	76(13)			
		4	1030.7(1)*	100(17)			
3499.8(2)*		2^+	2667.1(1)*	100(13)		0.40(5)	109(25)*
		4^+	1037.6(2)*	43(6)			
3514.7(2)*		4^+	1996.5(2)*	100			
3522.2(2)*		2^+	2689.7(1)*	100		0.57(4)	53(10)
3597.3(2)*		2^+	2764.8(1)*	100			

[a]Adopted from [51].
[b]Adopted from NNDC database.
[c]Adopted from [49].
[d]No reliable photopeak efficiency has been obtained for $E_\gamma < 200$ keV.
[e]Adopted from [19].
[f]Adopted from [20].

the experimental results for several excited states that are either of particular interest for the discussion in Sec. IV or of those whose experimental observables are in conflict with previous experiments.

1931 keV level. A γ-decay of this level to the ground state was reported in [19] which is not confirmed from our present data. From the present experiment, an upper limit for the γ-decay branching ratio of 0.5% was extracted for the ground-state transition, which is considerably smaller compared to the previously reported value of 6(1)% [19]. The new measured level lifetime of 395^{+47}_{-43} fs is smaller compared to the value reported in a previous measurement [49], but agrees within the experimental uncertainties. The error of the lifetime value is reduced by a factor of four. The obtained multipole mixing ratio of $\delta = -1.1(2)$ is in agreement with a previous measurement [19].

2283 keV level. The 2^+_3 state at 2283 keV has been previously identified as the one-phonon quadrupole mixed-symmetry state $2^+_{1,\mathrm{ms}}$ based on the measurement of absolute $M1$ and $E2$ transition strengths [18]. The multipole mixing ratio for the γ decay to the 2^+_1 state of $\delta = 0.01(5)$ extracted in this experiment [see Fig. 2(b)] is smaller than the value of $\delta = 0.12(3)$ quoted in Ref. [19]; however, it agrees with the value of $\delta = 0.03(10)$ reported in Ref. [48]. In any case, all measurements agree on a dominant $M1$ character of the $2^+_3 \to 2^+_1$ transition. In our previous article [29] a lifetime value of $\tau = 25(3)$ fs was used to calculate the transition strengths quoted therein. Because of an improved error analysis, we slightly revise the value to $\tau = 23(2)$ fs. The level lifetime is in excellent agreement with a previously measured value of $\tau = 22(7)$ fs [18]. A new γ decay branching to the 2^+_2 state at 1931 keV has been observed in this work. The low γ-ray energy of 352 keV suggests a dominant $M1$ character for this transition.

2462 keV level. Based on the observation of a new γ-ray transition from this $J = 4$ level to the 2^+_1 state, a positive parity was assigned. The lifetime value of $\tau = 72(5)$ fs [see Fig. 3(c)] obtained in this measurement is about a factor of 2 lower compared to the one reported in [49]; however, it still agrees within the uncertainties. The obtained multipole mixing ratio of $\delta = -0.19(10)$ indicates a dominant $M1$ character for the $4^+_2 \to 4^+_1$ transition [see Fig. 2(c)].

2740 keV level. On the basis of its γ-decay branching ratios, this state has been previously interpreted as the 2^+ member of the $(2^+_{1,\mathrm{ms}} \otimes 2^+_{1,\mathrm{s}})$ quintuplet [19]. In this work we extracted the multipole-mixing ratios for the transition to the 2^+_1 ($\delta = 3^{+4}_{-1}$) and 2^+_2 ($\delta = -0.01(9)$) states, indicating dominant $E2$ and $M1$ characters, respectively. The extracted lifetime of $\tau = 444(37)$ fs is in agreement with a previously quoted upper limit of 0.58 ps [19]. A weak γ decay branching to the ground state has been observed in this work for the first time.

2898 keV level. This state has been previously assigned as the 3^+ member of the $(2^+_{1,\mathrm{ms}} \otimes 2^+_{1,\mathrm{s}})$ quintuplet [19]. For the decay to the 2^+_2 state a multipole mixing ratio of $\delta = 0.07(4)$ was obtained for the first time. The extracted lifetime of $\tau = 432^{+48}_{-46}$ fs is in agreement with the upper limit of 0.58 ps which was reported in [19]. However, the deduced branching ratios are in conflict with previous results [19]. While the relative intensities for the decays to the 4^+_1 and 2^+_3 states are factors of 2 and 3 weaker, respectively, the branching ratio for the decay to the 4^+_2 state is larger by a factor of 4. Since the branching ratios obtained from the present $(p,p'\gamma)$ experiments at IKP Cologne and WNSL are in agreement within the quoted uncertainties, a systematic error, e.g., stemming from perturbed $p\gamma$-angular correlations, is unlikely. Possible contributions from other γ-ray transitions to the peak intensities were excluded on the basis of the $\gamma\gamma$ coincidence data. Hence, we revise the γ-decay branching ratios quoted in Ref. [19].

3076 keV level. For this state, a negative parity had been assigned based on the observation of a γ decay to the 5^- state at $E_x = 2588$ keV [49]. As in Ref. [19], this γ decay was not confirmed in the present experiments, so that a positive parity cannot be ruled out. However, the excitation energy of this level is close to known 3^- states of ^{92}Zr and ^{94}Mo [14,15] at 3040 keV and 3011 keV, respectively. Hence, a negative parity is tentatively assigned since no other possible $J^\pi = 3^-$ state is found up to an excitation energy of 3.4 MeV. A lifetime of

$\tau = 0.73(12)$ ps and a multipole mixing ratio of $\delta = -0.2(3)$ for the decay to the $3_1^{(-)}$ state were extracted from the present data for the first time.

3154 keV level. A $(2^+_{1,\mathrm{ms}} \otimes 2^+_{1,\mathrm{s}})_{1^+}$ character was proposed for this $J = 1$ state due to a tentatively assigned positive parity [20]. The newly measured value for the lifetime of $\tau = 9(2)$ fs is almost a factor of 2 larger compared to the value obtained from a previous (γ,γ') experiment [20]; however, it still agrees within the uncertainties. The γ-decay branching ratio for the decay of this level to the 2_2^+ state is found to be a factor of 2 smaller compared to the (γ,γ') results [20].

3282 keV level. Based on a tentatively assigned negative parity, this state was proposed to be the 1^- member of the $(2_1^+ \otimes 3_1^-)$ quintuplet [20]. Two new γ-decay transitions to the 2_1^+ and 0_2^+ states were obtained with relative intensities of 42(6)% and 9.4(17)%, respectively. The extracted lifetime of $\tau = 37(6)$ fs is in excellent agreement with the value obtained in a (γ,γ') experiment [20], when taking into account these new decay branching ratios.

IV. DISCUSSION

A. Coupling of symmetric quadrupole and octupole phonons

The coupling of the symmetric quadrupole and octupole phonons $(2_1^+ \otimes 3_1^-)$ results in a quintuplet with spin and parity quantum numbers $J^\pi = 1^- - 5^-$ [52]. The coupling of two nonidentical phonons is of particular interest since one expects a high degree of harmonicity due to the reduced Pauli blocking compared to, e.g., the coupling of two symmetric quadrupole phonons. For the nucleus ^{96}Ru, the center of gravity of the multiplet is expected around an excitation energy of $E(3_1^-) + E(2_1^+) = 3482$ keV.

Signatures for the two-phonon character are transitions to the constituent phonons, i.e., the symmetric one-phonon quadrupole and octupole states with transition strengths equal to the $B(E3; 3_1^- \to 0^+_{\mathrm{g.s.}})$ and $B(E2; 2_1^+ \to 0^+_{\mathrm{g.s.}})$ values, respectively [53,54]. In addition, a rather strong $E1$ ground-state transition has been observed for the 1^- member of the quintuplet [55].

From a previous (γ,γ') experiment, the $1_1^\pm$ state at $E_x = 3282$ keV has been proposed as a candidate for the 1^- member of the quintuplet despite missing parity information [20]. Unfortunately, a possible γ decay to the $3_1^{(-)}$ state was not observed in the present experiments due to the intense $6_1^+ \to 4_1^+$ yrast-band transition, which is close in energy to a hypothetical $1_1^\pm \to 3_1^{(-)}$ transition. However, a γ decay to the 2_1^+ state was observed in addition to the previously known ground-state transition. In a simple phonon picture, the ratio of the $B(E1)$ strength to the ground state and the $B(E1; 3_1^- \to 2_1^+)$ value is expected to be 7/3 if a two-phonon $E1$ operator is considered [56]. With values of $B(E1; 3_1^{(-)} \to 2_1^+) = 0.099(17)$ mW.u. and $B(E1; 1_1^\pm \to 0^+_{\mathrm{g.s.}}) = 0.24(6)$ mW.u., this is in excellent agreement with the phonon-picture estimate and supports the quadrupole-octupole coupled structure of the $1_1^\pm$ state. However, if a negative parity is assumed for the $J = 1^\pm$ state at $E_x = 3480$ keV, a ground-state transition strength of 0.21 mW.u. is obtained which results in a similar value for the $B(E1)$ ratio. Nevertheless, for most even-even nuclei where candidates for the $J^\pi = 1^-$ member of the quintuplet have been proposed, the excitation energy has been found to be systematically lower by about 5–10% compared to the sum energy of the constituent phonons [57,58]. Thus, it is more likely that the state at $E_x = 3282$ keV represents the main fragment of the $(2_1^+ \otimes 3_1^-)_{1^-}$ state of ^{96}Ru. However, an experiment aiming for the parity determination of the dipole excitations would be desirable to clarify their structure. For the dipole excitation at $E_x = 3449$ keV a two-phonon character is unlikely since no transitions other than the decay to the ground state were observed.

In total there are four states with a γ-ray transition to the $3_1^{(-)}$ state. Because of the small multipole mixing ratios for their transitions to the $3_1^{(-)}$ state, the states at 3073 and 3076 keV can be excluded to be of quadrupole-octupole coupled structure, as well as the $J = 4$ state at 3060 keV due to its positive parity. The γ-decay properties of the newly assigned state at $E_x = 3398$ keV agree with the expectations for a quadrupole-octupole coupled state, and therefore this state is a candidate for the 3^- member of the quintuplet. However, a spin and parity assignment is missing for a firm identification.

B. One- and two-phonon mixed-symmetry quadrupole excitations

The 2_3^+ state of ^{96}Ru at $E_x = 2283$ keV has been previously identified as the one-phonon mixed-symmetry quadrupole state $2^+_{1,\mathrm{ms}}$ based on the particular combination of a strong $M1$ transition to the 2_1^+ state and a weakly collective $E2$ transition to the ground state [18]. The transition strengths of $B(M1; 2_3^+ \to 2_1^+) = 0.75(14)\,\mu_N^2$ and $B(E2; 2_3^+ \to 0_1^+) = 1.5(3)$ W.u. obtained in this work are in excellent agreement with the previously reported values [18] and confirm the $2^+_{1,\mathrm{ms}}$ assignment. However, the uncertainty of the $B(M1)$ strength was reduced by almost a factor of 2.

The new data allow for a comprehensive study of the $M1$ strength distribution for decays to the 2_1^+ state; i.e., study of a possible fragmentation of the $2^+_{1,\mathrm{ms}}$ state. Figure 4(a) shows the obtained $M1$ strength distribution for transitions of low-lying 2^+ states to the 2_1^+ state, while the corresponding $E2$ strength distribution for decays to the ground state is shown in Fig. 4(b). The former is dominated by the $M1$ transition from the 2_3^+ state, while the transition from any other 2^+ state is weaker by almost one order of magnitude. In particular, no other 2^+ state shows decay characteristics similar to that of the 2_3^+ state. Thus, no considerable fragmentation of the $2^+_{1,\mathrm{ms}}$ state is found in the case of ^{96}Ru.

In a simple phonon picture, a two-phonon quintuplet of $0^+ - 4^+$ states is expected from the coupling of symmetric and mixed-symmetric quadrupole phonons $2_1^+ \otimes 2^+_{1,\mathrm{ms}}$ at the sum energy of the constituent phonons; i.e., at $E(2_1^+) + E(2_3^+) = 3.1$ MeV. The 1^+, 2^+, and 3^+ members of the quintuplet are expected to decay via $M1$ transitions to the symmetric two-phonon 2^+ state with transition strengths comparable to that of the $2^+_{1,\mathrm{ms}} \to 2^+_{1,\mathrm{s}}$ transition. Along with the $M1$ fingerprint, a weakly collective $E2$ transition to the symmetric one-phonon state is expected with a transition strengths comparable to that of the $2^+_{1,\mathrm{ms}} \to 0^+_{\mathrm{g.s.}}$ transition.

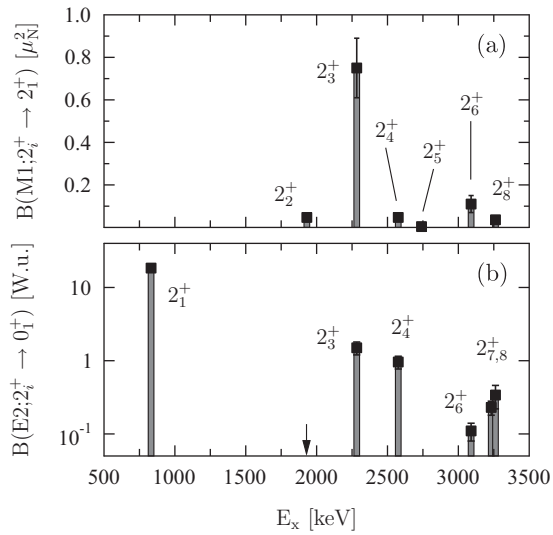

FIG. 4. The upper panel shows the measured $M1$ strengths distribution for the decay of low-lying non-yrast 2^+ states to the 2_1^+ state. The corresponding $E2$ transition strengths to the ground state are shown in the lower panel. Arrows mark transitions with strengths smaller than 0.05 W.u. Because of its characteristic decay properties, the 2_3^+ state represents a good realization of the one-phonon mixed-symmetry quadrupole excitation.

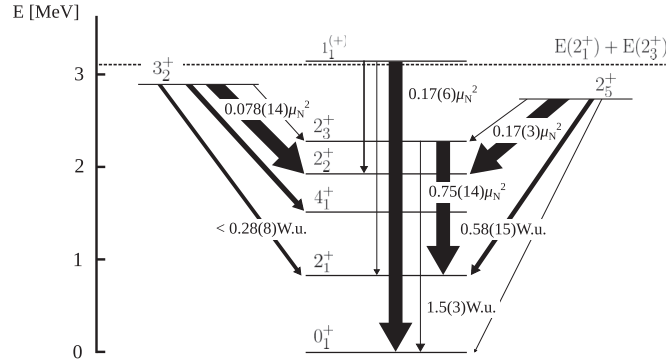

FIG. 5. Decay properties of candidates for the 1^+, 2^+, and 3^+ members of two-phonon mixed-symmetry quintuplet. The thickness of the arrows corresponds to the measured γ-decay intensities. If available, the measured $M1$ and $E2$ transition strengths are quoted as well. $M1$ transitions are indicated with the unit μ_N^2, while $E2$ transitions are quoted in W.u. The dashed horizontal line indicates the sum of the excitation energies of the 2_1^+ and 2_3^+ states.

In a previous study, the 2_5^+ and 3_2^+ states at excitation energies of 2740 and 2898 keV, respectively, have been proposed to be members of the two-phonon quintuplet [19]. The assignments were based on the similarity of the γ-decay branching ratios to the well established 2^+ and 3^+ members of the two-phonon mixed-symmetry quintuplet in ^{94}Mo [12,13]. However, no multipole mixing ratios and only upper limits for lifetime values were reported, so that a firm identification on the basis of reduced transition strengths was missing. The new experimental data obtained in this work allowed for a determination of transition strengths for the de-excitation of the 2_5^+ and 3_2^+ states. The decay properties of the 2_3^+, 2_5^+, 3_2^+, and $1_1^{(+)}$ states of ^{96}Ru are shown in Fig. 5, including the reduced transition strengths for transitions to lower-lying states. For the $2_5^+ \rightarrow 2_2^+$ transition an $M1$ strength of $0.17(3)\,\mu_N^2$ is obtained along with an $E2$ transition strength of 0.58(15) W.u. for the decay to the 2_1^+ state, supporting the $2_{2,\mathrm{ms}}^+$ assignment of the 2_5^+ state.

For the 3_2^+ state, only a small $M1$ transition strength of $0.078(14)\,\mu_N^2$ is obtained for the decay to the 2_2^+ state. This is about one order of magnitude weaker compared to the $B(M1; 2_{1,\mathrm{ms}}^+ \rightarrow 2_1^+)$ value and a factor of 3 weaker compared to the $3_{\mathrm{ms}}^+ \rightarrow 2_2^+$ transition of ^{94}Mo [14]. However, the transition is of dominant $M1$ character, and the transition matrix element of $\langle 3_2^+ || \hat{T}(M1) || 2_2^+ \rangle = 0.74(7)\ \mu_N$ does not exclude a mixed-symmetry character. A possible explanation of the decrease of $M1$ strength might be a fragmentation of the 3_{ms}^+ state. Indeed another $J = 3$ state is located close in energy at $E_x = 2851$ keV. In Ref. [19], this state was rejected to be the 3_{ms}^+ state, based on its different γ-decay properties compared to the 3_{ms}^+ state of ^{94}Mo. Unfortunately, no multipole mixing ratios could be extracted in this work for the transition to the 2_2^+ state. Assuming a pure $M1$ character, a transition strength of $0.086(16)\,\mu_N^2$ is obtained which is of comparable size to the $B(M1; 3_2^+ \rightarrow 2_2^+)$ value.

It has to be emphasized that also the $B(M1; 2_5^+ \rightarrow 2_2^+)$ value is only 30% of the $2_{1,\mathrm{ms}}^+ \rightarrow 2_1^+$ $M1$ transition strength and about 40% weaker than the $B(M1; 2_{2,\mathrm{ms}}^+ \rightarrow 2_2^+)$ value for ^{94}Mo [14]. Thus, a fragmentation of the $2_{2,\mathrm{ms}}^+$ cannot be excluded as well. However, this cannot be studied on the basis of the present experimental data due to a lack of experimental multipole mixing ratios for $2_i^+ \rightarrow 2_2^+$ $(i > 2)$ transitions.

A candidate for the 1_{ms}^+ was obtained from a (γ,γ') experiment, based on its excitation energy of $E_x = 3154$ keV and a tentatively assigned positive parity [20]. Neither in the (γ,γ') experiment nor in the present experiments was a γ-decay branching to the $2_{1,\mathrm{ms}}^+$ state observed for any of the dipole excitations, as is the case for, e.g., the 1_{ms}^+ state of the neighboring nucleus ^{94}Mo. Moreover, no parity information was extracted from the present experiments, so that a firm identification of the 1_{ms}^+ state of ^{96}Ru is still missing.

C. One-phonon mixed-symmetry octupole excitations

Strong $M1$ transitions to their fully-symmetric counterparts are a fingerprint of mixed-symmetry states. Thus, strong $M1$ transitions to the lowest-lying 3_1^- state, which is usually interpreted as the symmetric one-phonon octupole vibrational state, have been regarded as evidence for mixed-symmetry octupole excitations [25]. In addition, strong F-vector $E1$ transitions to the 2_1^+ state are predicted in the $U_{\pi\nu}(1) \otimes U_{\pi\nu}(5) \otimes U_{\pi\nu}(7)$ limit of the sdf-IBM-2, according to the two-body nature of the $E1$ transition operator [27,28].

In ^{96}Ru, the $3_2^{(-)}$ state was found at an excitation energy of 3076 keV. This is close to the excitation energies of the proposed 3_{ms}^- candidates of ^{92}Zr and ^{94}Mo. Assuming a negative parity for the $3_2^{(-)}$ state, a transition strength of $B(M1; 3_2^{(-)} \rightarrow 3_1^-) = 0.14(4)\,\mu_N^2$ is obtained. Thus, this state

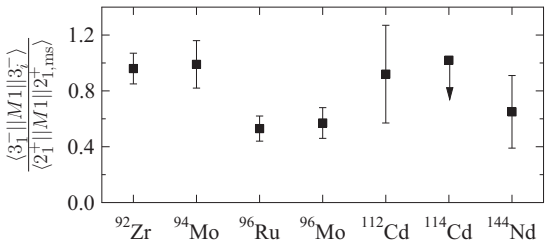

FIG. 6. Ratio of the $\langle 3_1^-||M1||3_i^-\rangle$ and $\langle 2_{1,s}^+||M1||2_{1,ms}^+\rangle$ matrix elements for nuclei in the $A \approx 100$ mass region and for ^{144}Nd. The ratio for ^{96}Ru is a factor of 2 lower compared to the other $N = 52$ isotones ^{92}Zr and ^{94}Mo, but close to the value for ^{96}Mo. For ^{114}Cd, only an upper limit has been reported up to now. The data, except for ^{96}Ru, are adopted from [25].

is a likely candidate for the one-phonon mixed-symmetry octupole state. Similar to ^{94}Mo, a sizable $E1$ strength of $B(E1) = 0.14(3)$ mW.u. was obtained for the decay to the one-phonon quadrupole mixed-symmetry state. However, only a small $E1$ strength of $B(E1; 3_2^{(-)} \rightarrow 2_1^+) = 0.0017(3)$ mW.u. is obtained for the decay to the symmetric one-phonon quadrupole state, which is in conflict with the sdf-IBM-2 prediction.

In the $U_{\pi\nu}(1) \otimes U_{\pi\nu}(5) \otimes U_{\pi\nu}(7)$ limit of the sdf-IBM-2, the reduced transition strength of the $3_{ms}^- \rightarrow 3_1^-$ transition can be calculated analytically [27]:

$$B(M1; 3_{ms}^- \rightarrow 3_1^-) = \frac{9}{\pi}(g_\pi - g_\nu)^2 \frac{N_\pi N_\nu}{N^2} \qquad (2)$$

with g_π and g_ν being the proton and neutron g factors for the f bosons and N_π, N_ν, and N, the proton, neutron, and total boson numbers, respectively. Assuming ^{100}Sn as inert core gives $N_\pi = 3$ and $N_\nu = 1$. With the bare orbital g factors for protons and neutrons ($g_\pi = 1$ and $g_\nu = 0$), a reduced $M1$ transition strength of 0.54 μ_N^2 is predicted, which is almost a factor of 4 larger compared to the experimental value. Note that the same value is obtained if ^{88}Sr is assumed as inert core.

As discussed in Ref. [25], the $\langle 3_1^-||M1||3_2^{(-)}\rangle$ matrix element is expected to scale with the one for the $2_{1,ms}^+ \rightarrow 2_{1,s}^+$ transition if a 3_{ms}^- character is assumed for the $3_2^{(-)}$ state. With the bare orbital g factors, the sdf-IBM-2 predicts a value of $\sqrt{14/5} \approx 1.67$ for the ratio of their absolute values. From the present data, an experimental ratio of $\frac{\langle 3_1^-||M1||3_2^{(-)}\rangle}{\langle 2_s^+||M1||2_{ms}^+\rangle} = 0.53(9)$ was obtained which is about a factor of 3 smaller compared to the predicted value. Figure 6 shows this value for ^{96}Ru in comparison to the other $A \approx 100$ nuclei that were investigated with respect to mixed-symmetry octupole excitations in Ref. [25]. Among others also the $N = 52$ isotones ^{92}Zr and ^{94}Mo are shown. The present value is about a factor of 2 smaller compared to the lighter $N = 52$ isotones, but close to the value for ^{96}Mo. The reduced value for ^{96}Ru compared to the other $N = 52$ isotones might result from a fragmentation of the mixed-symmetry octupole excitation, a less collective nature of the $M1$ transition in the case of ^{96}Ru, or the more $O(6)$-like structure of ^{96}Ru compared to, e.g., ^{94}Mo (see Sec. V).

D. One-phonon mixed-symmetry hexadecapole excitations

Based on the observation of strong $M1$ transitions connecting the lowest-lying 4^+ states in ^{94}Mo and ^{92}Zr, one-phonon hexadecapole components of symmetric and mixed-symmetric character have been discussed to contribute to the wave functions of the 4_1^+ and 4_2^+ states, respectively [14,15,26]. In particular for the case of ^{94}Mo, the one-phonon hexadecapole assignment is supported by recent sdg-IBM-2 and shell-model calculations, the latter using a surface delta interaction (SDI) [26]. For ^{96}Ru, the 4_2^+ state is found at an excitation energy of $E_x = 2462$ keV. A transition strength of $B(M1) = 0.90(18)\,\mu_N^2$ is obtained for the transition to the 4_1^+ state which is comparable to the corresponding $M1$ transition strength of $B(M1) = 1.23(20)\,\mu_N^2$ found in ^{94}Mo. Thus, the strong $M1$ transition suggests symmetric and mixed-symmetry one-phonon hexadecapole components in the wave functions of the 4_1^+ and 4_2^+ states, respectively.

In the case of ^{94}Mo, strong $4_i^+ \rightarrow 4_1^+$ $M1$ transitions with $i > 2$ have been observed experimentally in addition to the $4_2^+ \rightarrow 4_1^+$ transition [14]. Unfortunately, the assignment of spins and multipole mixing ratios for higher lying 4^+ states and transitions to the 4_1^+ state in ^{96}Ru are ambiguous on the basis of the present experimental data, and thus a fragmentation of the corresponding $M1$ strength could not be analyzed.

V. *sdg*-IBM-2 CALCULATIONS

The sdg-IBM-2 calculations follow the approach of Ref. [26] for the description of ^{94}Mo. Technical details of the present calculation for the case of ^{96}Ru, such as the chosen Hamiltonian and transition operators as well as their adopted parameters, have already been discussed in a preceding article [29] and will not be repeated here. In the previous paper, the discussion focused on the interpretation of the observed strong $M1$ transition connecting the lowest-lying 4^+ states as an F-vector transition connecting mixed-symmetry and fully-symmetric states with one-phonon hexadecapole character. Indeed, this interpretation was supported by the calculations. In the present article, we restrict ourselves to the discussion of the sdg-IBM-2 results for the one- and two-phonon mixed-symmetry quadrupole excitations.

The results of the sdg-IBM-2 calculations are compiled in Table II for the low-lying $J^\pi = 0^+ - 4^+$ states. Except for the 0_2^+ and 2_5^+ states, the experimental level energies are reproduced within a deviation of less than 260 keV. Also the calculated transition strengths are in overall agreement with the experimental values.

From the calculated F-spin quantum numbers, a mixed-symmetry character is obtained for the 2_3^+, 2_5^+, 3_2^+, and 4_2^+ states. Experimentally, the 2_3^+ state was identified with the one-phonon quadrupole mixed-symmetry state, which is in agreement with the present calculations. The IBM calculations result in a dominant one-phonon character for this state with s- and d-boson contents similar to those of the symmetric one-phonon state. While the $M1$ transition strength for the decay to the 2_1^+ state is fixed in the calculation by the choice of the proton g factor, the weakly collective $E2$ transition to the ground state is reproduced by the calculation. However, the calculated value is larger by a factor of 2. Since the weakly

TABLE II. Results of the *sdg*-IBM-2 calculations in comparison to the experimental data. The experimental and calculated level energies (columns 2 and 3) are given in units of MeV. Columns 5, 6, and 7 show the calculated *s*-, *d*-, and *g*-boson contents in the IBM wave functions. In the last two columns, the reduced transition strengths are given. $M1$ strengths are quoted in units of μ_N^2; $E2$ strenghts are given in units of W.u.. The calculated F-spin quantum number is quoted in column 4. An F-spin quantum number of 2 corresponds to maximum F spin, i.e., a fully-symmetric character.

Level	Energies (MeV)		F	Boson numbers			Transition strengths [W.u. ($E2$) and μ_N^2 ($M1$)]			
	$E_{\rm exp}$	$E_{\rm IBM}$		$\langle n_s\rangle$	$\langle n_d\rangle$	$\langle n_g\rangle$	$J_i^\pi \to J_f^\pi$	$\sigma\lambda$	$B(\sigma\lambda)_{\rm exp}$	$B(\sigma\lambda)_{\rm IBM}$
0_1^+	0.000	0.000	2	3.4	0.3	0.0				
0_2^+	2.149	2.596	2	2.2	1.5	0.3	$0_2^+ \to 2_1^+$	$E2$	11.7(18)	7.7
1_1^+	3.154	2.944	1	1.7	1.8	0.5	$1_1^+ \to 0_1^+$	$M1$	0.17(6)	0.13
2_1^+	0.832	0.832	2	2.6	1.3	0.1	$2_1^+ \to 0_1^+$	$E2$	18.1(5)	18.4
2_2^+	1.932	2.165	2	1.8	2.0	0.2	$2_2^+ \to 2_1^+$	$M1$	0.05(2)	0
							$2_2^+ \to 2_1^+$	$E2$	28(9)	24
2_3^+	2.283	2.322	1	2.5	1.2	0.3	$2_3^+ \to 2_1^+$	$M1$	0.75(14)	0.69
							$2_3^+ \to 0_1^+$	$E2$	1.5(3)	2.53
2_5^+	2.740	3.637	1	1.7	1.8	0.5	$2_5^+ \to 0_1^+$	$E2$	0.006(12)	0
							$2_5^+ \to 2_1^+$	$E2$	0.58(15)	1.92
							$2_5^+ \to 2_2^+$	$M1$	0.17(3)	0.17
3_1^+	2.852	3.072	2	1.7	1.5	0.8	$3_1^+ \to 2_1^+$	$E2$	<0.01	0
							$3_1^+ \to 2_1^+$	$M1$	0.008(1)	0
							$3_1^+ \to 2_2^+$	$E2$	<5.58	14.7
3_2^+	2.898	3.158	1	1.7	1.9	0.4	$3_2^+ \to 2_1^+$	$E2$	<0.28	3.17
							$3_2^+ \to 2_2^+$	$E2$	0.02(4)	0
							$3_2^+ \to 2_2^+$	$M1$	0.078(14)	0.563
4_1^+	1.518	1.523	2	2.3	1.2	0.6	$4_1^+ \to 2_1^+$	$E2$	22.6(17)	25.6
4_2^+	2.462	2.482	1	2.6	0.5	0.9	$4_2^+ \to 4_1^+$	$M1$	0.90(18)	1.13
							$4_2^+ \to 2_1^+$	$E2$	1.52(19)	1.44

collective $E2$ transition stems from a destructive interference of proton and neutron contributions in the $E2$ transition operator, this might be improved by adjusting the adopted value for proton and neutron effective charges, however, at the cost of an additional free parameter in the calculation.

A two-phonon quadrupole mixed-symmetry character is predicted for the 1_2^+, 2_5^+, and 3_2^+ states. This is reflected in their *d*-boson contributions that are enhanced by about 30% compared to the one-phonon quadrupole excitations. However, they are similar to that of the 0_2^+ and 2_2^+ states which are the symmetric two-phonon states. The excitation energy of the 2_5^+ state is overestimated by almost 1 MeV, but the transition strength for its decay to the 2_2^+ state is in agreement with the data. As it is the case for the 2_3^+ state, the weakly collective $E2$ transition to the 2_1^+ state is overestimated by a factor of 3.

For the 3_2^+ state, a strong $M1$ transition to the 2_2^+ state is predicted along with a weakly collective $E2$ transition to the 2_1^+ state, as expected for a two-phonon mixed-symmetry state. However, the experimental value is smaller by almost one order of magnitude. Also the small $E2$ transition to the 2_1^+ state is not described by the calculations. For the 3_1^+ state, a dominant $(g^\dagger d^\dagger)^{(3)}$-boson structure is predicted, reflected by the vanishing $E2$ transition strength to the 2_1^+ state because of *d*-parity conservation rules [59] and its enhanced *g*-boson contribution.

VI. SHELL-MODEL CALCULATIONS

Several shell-model (SM) studies have been previously performed in the $A \approx 100$ mass region to describe the experimentally observed properties of mixed-symmetry states. The calculations focused on a description of the $N = 52$ nuclei ^{92}Zr [16], ^{94}Mo [8], and ^{96}Ru [19], using two-body matrix elements (TBMEs) obtained from a surface delta interaction (SDI). Moreover, calculations for the whole $N = 52$ isotonic chain have been performed using a $V_{\rm low\text{-}k}$ interaction [60]. Additional studies have been carried out for neutron-deficient Cd isotopes [61] as well as for Zr isotopes [62].

The purpose of the present study is to obtain a microscopic interpretation of the observed strong $4_2^+ \to 4_1^+$ $M1$ transition strength. While the *sdg*-IBM-2 calculations support the interpretation of an isovector $M1$ transition connecting mixed-symmetric and fully-symmetric states, the large $M1$ transition matrix element might also be explained by the underlying microscopic structure: if similar single-particle configurations with large *g* factors are assumed to be present in the wave functions of the 4_1^+ and 4_2^+ states, this might result in a strong $4_2^+ \to 4_1^+$ transition as well. On the other hand, contributions from $d_{5/2} \leftrightarrow d_{3/2}$ spin-flip transitions might also account for the large $B(M1; 4_2^+ \to 4_1^+)$ values that

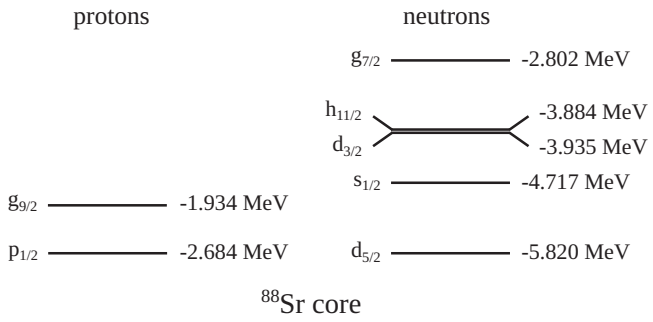

FIG. 7. Model space used for the present SM calculations. The single-particle energies for the proton (left) and neutron orbits (right) relative to the ^{88}Sr core are adopted from Ref. [63].

have been experimentally observed for all stable, even-even $N = 52$ isotones. Because of their microscopic character, these interpretations are beyond the scope of *sdg*-IBM-2 calculations. In order to examine these possibilities, the present shell-model calculations aim for an investigation of the proton-neutron symmetry of the wave functions of low-lying 2^+ and 4^+ states.

The SM calculations were performed with the m-scheme code NUSHELL@MSU [64]. The model space for a ^{88}Sr core included the proton orbitals $p_{1/2}$ and $g_{9/2}$ as well as the neutron orbitals $d_{5/2}$, $g_{7/2}$, $s_{1/2}$, $d_{3/2}$, and $h_{11/2}$. The single-particle energies (SPEs) were adopted from Ref. [63], where they were fixed to reproduce the extrapolated values for a ^{100}Sn core [65]. The model space and the corresponding SPEs are depicted in Fig. 7. TBMEs were obtained from an effective interaction that was derived by employing a pertubative many-body scheme starting from the free nucleon-nucleon interaction as described in Ref. [66]. This interaction has been previously used to study Gamow-Teller (GT) strength in ^{100}Cd [63] and for the description of ^{98,100}Pd nuclei [67–69]. To adjust the proton and neutron effective charges e_π and e_ν, a method was applied that takes advantage of the different proton-neutron symmetries of the wave functions of the $2^+_{1,\mathrm{ms}}$ and $2^+_{1,\mathrm{s}}$ states. Instead of adjusting the proton and neutron effective charges e_π and e_ν separately, the isoscalar and isovector effective charges $e_{\mathrm{IS}} = \frac{1}{2}(e_\pi + e_\nu)$ and $e_{\mathrm{IV}} = \frac{1}{2}(e_\pi - e_\nu)$ were varied to simultaneously describe the experimental $B(E2; 2^+_1 \to 0^+_1)$ and $B(E2; 2^+_3 \to 0^+_1)$ values. Following this approach, as described in more detail below, we obtained the effective charges of $e_\pi = 2.215e$ and $e_\nu = 0.661e$ used for the present calculation. For the spin g factors we applied a quenching factor of $\alpha = 0.57$ in order to obtain pure isovector $M1$ transitions [8].

The level scheme and transition strengths calculated with the SM are shown in Fig. 8 and Table III, respectively, in comparison to experiment and the results of the *sdg*-IBM-2 calculations. The SM low-lying level scheme is in good agreement with the experimental one. However, a few deviations are observed above an excitation energy of 2 MeV: the calculated 4^+_3 state is found at an excitation energy similar to the experimental 4^+_2 state. In addition, the largest $M1$ transition strength to the 4^+_1 state is calculated for the deexcitation of the 4^+_3 level. The SM calculation does not predict any other 4^+

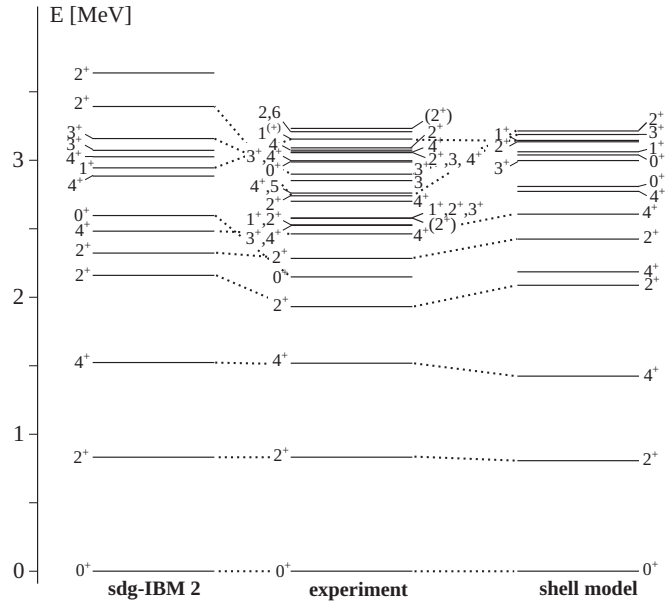

FIG. 8. Comparison of the experimental level scheme (middle) with the results of the *sdg*-IBM-2 (left) and shell-model calculations (right). In the cases where a one-to-one correspondence of the experimental and calculated states on the basis of similar decay properties was obtained, they are connected with dashed lines.

TABLE III. Experimental reduced $E2$ and $M1$ transition strengths compared with the results from SM and *sdg*-IBM-2 calculations. $E2$ strengths are given in units of W.u., $M1$ transitions are quoted in μ_N^2. If not indicated differently, the experimental values are obtained from this work.

Transition	Experiment	SM	*sdg*-IBM-2
$B(E2; 2^+_1 \to 0^+_1)$	18.1(5)[a]	18.1	18.4
$B(E2; 0^+_2 \to 2^+_1)$	11.7(18)	2.6	7.7
$B(E2; 2^+_2 \to 0^+_1)$	<0.002	0.95	0
$B(E2; 2^+_2 \to 2^+_1)$	28(9)	19	24
$B(E2; 2^+_3 \to 0^+_1)$	1.5(3)	1.5	2.53
$B(E2; 2^+_5 \to 2^+_1)$	0.58(15)	0.22[b]	1.92
$B(E2; 3^+_2 \to 2^+_1)$	0.28(5)	2.17	3.2
$B(E2; 3^+_2 \to 2^+_2)$	0.2(4)	1.0	0
$B(E2; 4^+_1 \to 2^+_1)$	22.6(17)[a]	21.7	25.6
$B(E2; 4^+_2 \to 2^+_1)$	1.5(4)	1.1[c]	1.44
$B(M1; 1^+_1 \to 0^+_1)$	0.17(5)	0.08	0.13
$B(M1; 2^+_2 \to 2^+_1)$	0.05(2)	0.0012	0
$B(M1; 2^+_3 \to 2^+_1)$	0.75(14)	0.72	0.69
$B(M1; 2^+_5 \to 2^+_2)$	0.17(3)	0.44[b]	0.17
$B(M1; 2^+_5 \to 2^+_3)$	0.047(11)	0.137[b]	0
$B(M1; 3^+_2 \to 2^+_2)$	0.078(14)	0.265	0.563
$B(M1; 4^+_2 \to 4^+_1)$	0.90(18)	1.32[c]	1.13

[a]Adopted from Ref. [19].
[b]Value for the 2^+_4 SM state.
[c]Value for the 4^+_3 SM state.

state with a comparable transition strength. Because of their similar excitation energies and decay properties we identify the calculated 4_3^+ state to correspond to the experimental 4_2^+ state. Similarly, the calculated 2_4^+ state is the only 2^+ state above the 2_3^+ state with a considerable $B(M1)$ strength for a transition to the 2_2^+ state, and thus we identify the 2_4^+ SM state to be the experimental 2_5^+ state.

The transition strengths obtained from the SM calculations are in good agreement with the experimental data (see Table III). Note that only the $B(E2)$ values for the ground-state transitions of the 2_1^+ and 2_3^+ states were fixed to reproduce the experimental values. The calculated $B(M1; 2_3^+ \rightarrow 2_1^+)$ value is in excellent agreement with the experimental value and supports the assignment of the 2_3^+ state as the one-phonon mixed-symmetry quadrupole state (see discussion below). In contrast, the calculated $M1$ transition strength of $0.44\,\mu_N^2$ for the de-excitation of the 2^+ member of the two-phonon mixed-symmetry quintuplet to the symmetric two-phonon 2^+ state, i.e., the SM $2_4^+ \rightarrow 2_2^+$ transition, is overestimated by more than a factor of 2 compared to the experimental value and the sdg-IBM-2 prediction. Similarly, the calculated $B(M1)$ value of $0.265\,\mu_N^2$ for the $3_2^+ \rightarrow 2_2^+$ transition, which is the de-excitation of the $3_{1,\mathrm{ms}}^+$ state to the symmetric two-phonon 2^+ state, is larger by a factor of 3 compared to the data. However, the value obtained from the IBM calculations exceeds the experimental value by a factor of 7. The experimentally observed strong $E2$ strength of 11.7(18) W.u. for the $0_2^+ \rightarrow 2_1^+$ transition is not reproduced by the SM calculations but in fair agreement with the sdg-IBM-2 result.

As an important result, the strong $M1$ transition connecting the low-lying 4^+ states is reproduced by both calculations. Though the $M1$ transition strength calculated with the SM is about 40% larger compared to the experimental value, the correct order of magnitude is predicted without any additional adjustment of the $M1$ transition operator.

To investigate the proton-neutron symmetry (pn symmetry) of the calculated wave functions of 2^+ states, the $E2$ transition operator

$$\hat{T}(E2) = e_\pi \hat{T}_\pi(E2) + e_\nu \hat{T}_\nu(E2) \tag{3}$$

was decomposed into an isoscalar part

$$\hat{T}_{\mathrm{IS}}(E2) = e_{\mathrm{IS}}(\hat{T}_\pi(E2) + \hat{T}_\nu(E2)) \tag{4}$$

and an isovector part

$$\hat{T}_{\mathrm{IV}}(E2) = e_{\mathrm{IV}}(\hat{T}_\pi(E2) - \hat{T}_\nu(E2)). \tag{5}$$

Here, $\hat{T}_\rho(E2) = \sum_i (r_i^\rho)^2 \hat{Y}_2(\theta_i^\rho, \phi_i^\rho)$ are the proton ($\rho = \pi$) and neutron ($\rho = \nu$) parts of the $E2$ transition operator, e_ρ are the effective charges, and e_{IV} and e_{IS} can be expressed as $e_{\mathrm{IS}} = \frac{1}{2}(e_\pi + e_\nu)$ and $e_{\mathrm{IV}} = \frac{1}{2}(e_\pi - e_\nu)$, respectively.

The isovector contribution vanishes for transitions between two states with same, that is either pn-symmetric or mixed-symmetric wave functions, the latter denoting the case when the wave function is not symmetric under exchange of the pn labels of at least one proton-neutron pair. On the contrary, isoscalar contributions vanish for transitions between two states with opposite pn-symmetry [8,61]. With this decomposition, the $B(E2)$ strength between two states J_i^π, J_f^π can be written as

$$\begin{aligned} B\left(E2; J_i^\pi \rightarrow J_f^\pi\right) \propto\ & e_{\mathrm{IS}}^2 \left|\left\langle J_f^\pi \left\| \hat{T}_{\mathrm{IS}}(E2) \right\| J_i^\pi \right\rangle\right|^2 \\ & + 2\, e_{\mathrm{IS}}\, e_{\mathrm{IV}} \left|\left\langle J_f^\pi \left\| \hat{T}_{\mathrm{IS}}(E2) \right\| J_i^\pi \right\rangle \left\langle J_f^\pi \left\| \hat{T}_{\mathrm{IV}}(E2) \right\| J_i^\pi \right\rangle\right| \\ & + e_{\mathrm{IV}}^2 \left|\left\langle J_f^\pi \left\| \hat{T}_{\mathrm{IV}}(E2) \right\| J_i^\pi \right\rangle\right|^2. \end{aligned} \tag{6}$$

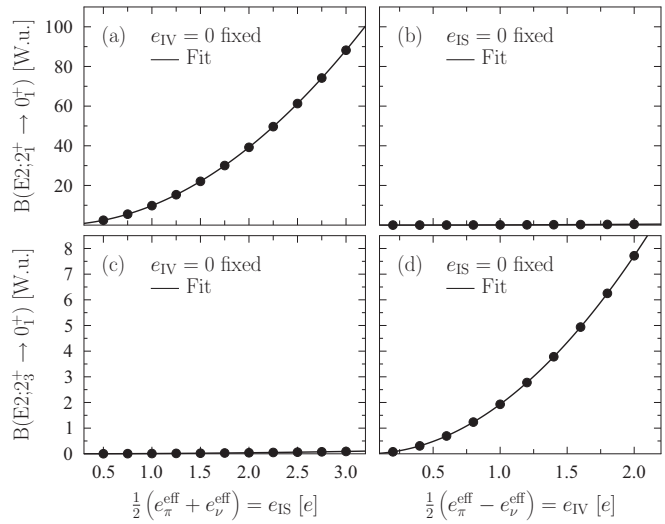

FIG. 9. Calculated $B(E2)$ strength of the ground-state transitions of the 2_1^+ (upper panel) and the 2_3^+ (lower panel) states as a function of the isoscalar (left) and isovector (right) effective charges. The respective other effective charge was fixed to zero. As suggested by Eq. (6), the calculated transition strengths are perfectly described by a fit with a second order polynomial (solid line). The correlation of the $2_1^+ \rightarrow 0_1^+$ and $2_3^+ \rightarrow 0_1^+$ transition strengths with the isoscalar and isovector effective charges, respectively, were used to fix the proton and neutron effective charges e_π and e_ν.

Thus, fixing one of the parameters, e_{IS} or e_{IV}, the $B(E2)$ strength is related to the other via a second order polynomial. For the ground-state transitions of the 2_1^+ and 2_3^+ states this is shown in Fig. 9 for fixed values of $e_{\mathrm{IS}} = 0$ or $e_{\mathrm{IV}} = 0$. A strong correlation of the $2_1^+ \rightarrow 0_1^+$ transition strength with the isoscalar effective charge is obtained, while the transition strength is very small and almost independent of a variation of the isovector effective charge. In contrast, the $2_3^+ \rightarrow 0_1^+$ transition strength is strongly correlated to the isovector effective charge and is almost independent of the isoscalar effective charge. This already indicates a pn-symmetric and mixed-symmetric character of the calculated wave functions of the 2_1^+ and 2_3^+ states, respectively, since the ground state is of pn-symmetric character.

This correlation of the ground-state transition strengths of the 2_1^+ and 2_3^+ states was used to adjust the effective charges e_{IS} and e_{IV}. The isoscalar (isovector) effective charge was fitted to reproduce the experimental $E2$ strength of the $2_1^+ \rightarrow 0_1^+$ ($2_3^+ \rightarrow 0_1^+$) transition, while the isovector (isoscalar) effective charge was fixed to zero. From the obtained values for e_{IS} and e_{IV}, the proton and neutron effective charges $e_\pi = e_{\mathrm{IS}} + e_{\mathrm{IV}}$ and $e_\nu = e_{\mathrm{IS}} - e_{\mathrm{IV}}$ were calculated.

Because of small admixtures of isovector and isoscalar components in the wave functions of the 2_1^+ and 2_3^+ SM

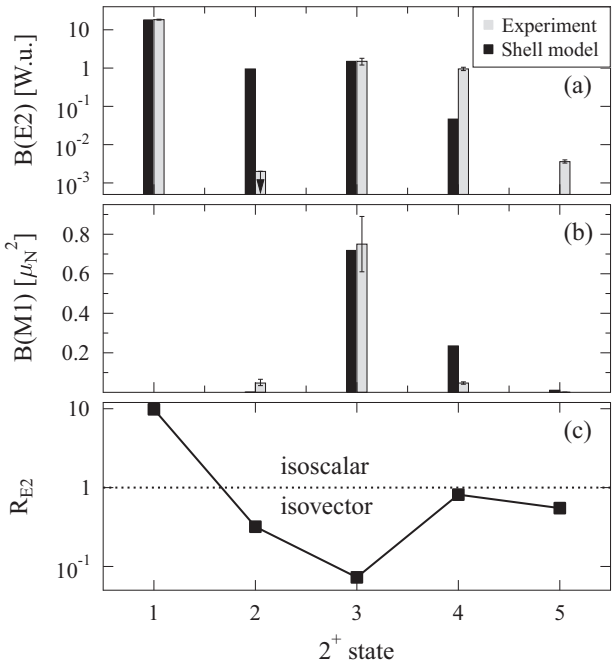

FIG. 10. Results of the shell-model calculations for the five lowest-lying 2^+ states. (a) The calculated $E2$ strengths to the ground state and (b) $M1$ strengths for the decay to the 2_1^+ state are compared to the experimental data. Arrows indicate upper limits for the corresponding transition strengths. Based on their γ-decay properties, the 2_1^+ and 2_3^+ states are identified to be the one-phonon symmetric and mixed-symmetry excitations, respectively. (c) The calculated values of R_{E2}, that are based on SM $B(E2)$ values, support the different proton-neutron symmetry of the wave functions of the 2_1^+ and 2_3^+ states. The dashed line separates the regions of dominant isovector and dominant isoscalar excitations from the ground state.

states, the experimental $E2$ strengths for of the $2_1^+ \to 0_1^+$ and $2_3^+ \to 0_1^+$ transitions are not exactly reproduced with the fitted effective charges obtained with the initial choice of $e_{IV} = 0$ and $e_{IS} = 0$, respectively. Therefore, the described fitting procedure was applied in an iterative way. Convergence on a percent level is obtained after a fifth step of iteration. As a final set of effective charges the above stated values of $e_\pi = 2.215e$ and $e_\nu = 0.661e$ were obtained. These values were adopted for the present SM calculation.

From Eq. (6), one obtains a ratio of isoscalar and isovector $E2$ transition matrix elements R_{E2} by choosing $J_f^\pi = 0_1^+$ as well as a combination of $e_{IS} = 1$ and $e_{IV} = 0$ and vice versa:

$$R_{E2} := \sqrt{\frac{B\left(E2; J_i^\pi \to 0_1^+; e_{IS} = 1, e_{IV} = 0\right)}{B\left(E2; J_i^\pi \to 0_1^+; e_{IS} = 0, e_{IV} = 1\right)}} = \left| \frac{\langle 0_1^+ | \hat{T}_{IS}(E2) | J_i^\pi \rangle}{\langle 0_1^+ | \hat{T}_{IV}(E2) | J_i^\pi \rangle} \right|. \quad (7)$$

Hence, the ratio R_{E2} allows for a quantitative measure of the pn-symmetry of the wave function of the state J_i^π relative to the ground state: if the state J_i^π is characterized by a pn-symmetric wave function, J_i^π will be connected to the ground state via a dominant isoscalar $E2$ transition, so that $R_{E2} > 1$, while $R_{E2} < 1$ is obtained if the state J_i^π corresponds to an isovector valence-shell excitation. Note the similarity of Eq. (7) to the quantity which is frequently used in QPM calculations to quantify the isospin nature of the QRPA-phonons; see, e.g., Refs. [70–72] and references therein.

TABLE IV. Ratios R_{E2} and R_{E4} of the isoscalar and isovector SM matrix elements of ground-state transitions of low-lying 2^+ and 4^+ states, respectively. The calculated ground-state transition strengths and the $M1$ strengths for the decay to the 2_1^+ and 4_1^+ states are shown as well. For the 2_3^+ and 4_3^+ shell-model states a dominant isovector ground-state transition is obtained along with a sizable $M1$ strengths to the 2_1^+ and 4_1^+ states, respectively.

J_i^π	$R_{E\lambda}$	$B(E\lambda; J_i^\pi \to 0_1^+)$ (W.u.)	$B(M1; J_i^\pi \to J_1^\pi)$ (μ_N^2)
2_1^+	9.8	18.1	
2_2^+	0.32	0.95	0.0012
2_3^+	0.073	1.50	0.72
2_4^+	0.81	0.047	0.24
2_5^+	0.55	3.2×10^{-5}	0.011
4_1^+	4.4	9.86	
4_2^+	1.3	7.20	3.0×10^{-4}
4_3^+	0.10	0.81	1.32
4_4^+	0.030	0.48	0.0024
4_5^+	0.086	0.33	0.095

Figure 10 and Table IV show the $B(E2)$ strengths of the five lowest-lying 2^+ states to the ground state [Fig. 10(a)], their $B(M1)$ strengths to the 2_1^+ state [Fig. 10(b)], and the ratio R_{E2} [Fig. 10(c)]. As expected from the discussion above, one obtains for the $2_1^+ \to 0_1^+$ transition a value of $R_{E2} = 9.8$ and, thus, a dominant pn-symmetric character of the 2_1^+ state. In contrast, a value of $R_{E2} = 0.073$ indicates a dominant isovector character for the weakly-collective ground-state transition of the 2_3^+ state. Along with the strong $2_3^+ \to 2_1^+$ $M1$ transition, this manifests the one-phonon quadrupole mixed-symmetry character of the calculated 2_3^+ state.

In the same way as discussed for the $E2$ transition operator, the $E4$ transition operator

$$\hat{T}(E4) = e_\pi \hat{T}_\pi(E4) + e_\nu \hat{T}_\nu(E4) \quad (8)$$

with $\hat{T}_\rho(E4) = \sum_i (r_i^\rho)^4 \hat{Y}_4(\theta_i^\rho, \phi_i^\rho)$, can be decomposed into an isoscalar and an isovector part, too. Thus, the ratio of the isoscalar and isovector transition matrix elements,

$$R_{E4} := \left| \frac{\langle 0_1^+ | \hat{T}_{IS}(E4) | J_i^\pi \rangle}{\langle 0_1^+ | \hat{T}_{IV}(E4) | J_i^\pi \rangle} \right|, \quad (9)$$

was calculated to investigate the proton-neutron symmetry of the wave functions of low-lying 4^+ states. Similar to the 2^+ states, the results are compiled in Fig. 11 and Table IV. A dominant isoscalar character is predicted for the $B(E4)$ ground-state transition of the 4_1^+ state ($R_{E4} = 4.4$). This indicates a proton-neutron symmetric wave function

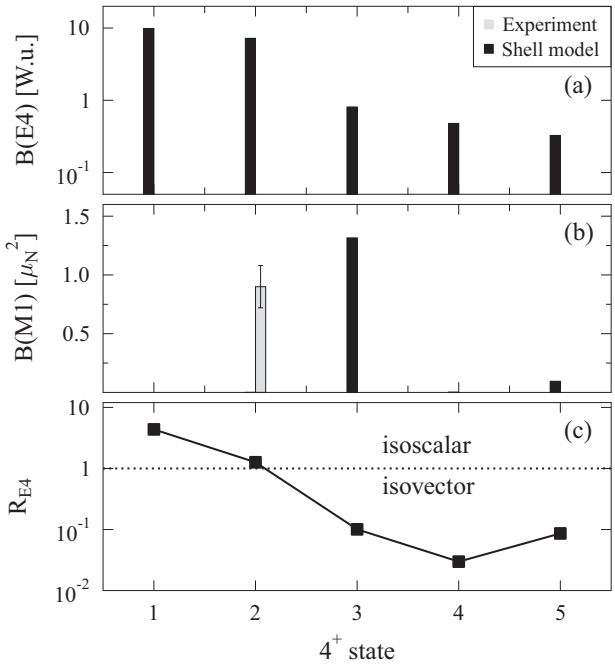

FIG. 11. Same as Fig. 10, but for the five lowest-lying 4^+ states. While the 4_1^+ state shows signatures of a symmetric one-phonon hexadecapole configuration, the γ-decay properties and the ratio R_{E4} hint toward a one-phonon hexadecapole configuration with mixed proton-neutron symmetry for the 4_3^+ shell-model state, which we assign to the experimental 4_2^+ state.

of the 4_1^+ state which is supported by the large calculated $B(E4; 4_1^+ \rightarrow 0_1^+)$ value of 9.86 W.u..

As already discussed, we identify the experimental 4_2^+ state to be the calculated 4_3^+ state because of its $M1$ decay properties. Thus, in Fig. 11(b) one should compare $B(M1; 4_2^+ \rightarrow 4_1^+)_{\text{exp}}$ with $B(M1; 4_3^+ \rightarrow 4_1^+)_{\text{SM}}$. Note the small calculated $B(M1; 4_2^+ \rightarrow 4_1^+)$ value of $3.0 \times 10^{-4}\,\mu_N^2$. For the SM 4_3^+ state, a dominant isovector character is obtained from the calculation ($R_{E4} = 0.10$). Along with the large $B(M1)$ transition strength to the 4_1^+ state and the weakly collective ground-state transition, this SM state matches the properties expected for a one-phonon hexadecapole mixed-symmetry state in terms of decay properties and proton-neutron symmetry. In addition, the similarity to the one-phonon mixed-symmetry state in the quadrupole sector is striking. We note that even smaller values for R_{E4} are obtained for the 4_4^+ and 4_5^+ states. However, their calculated $B(M1)$ transition strengths to the 4_1^+ state are at least one order of magnitude smaller compared to the calculated 4_3^+ state, and thus can be excluded as being a dominant fraction of the one-phonon hexadecapole mixed-symmetry state.

VII. COMPARISON TO ^{92}Zr AND ^{94}Mo

With the new experimental data on one- and two-phonon mixed-symmetry states, we perform a comparison of mixed-symmetry states of ^{96}Ru to the ones of the neighboring $N = 52$ isotones ^{92}Zr and ^{94}Mo. In the case of ^{92}Zr, the $Z = 40$ subshell closure leads to a dominant neutron configuration

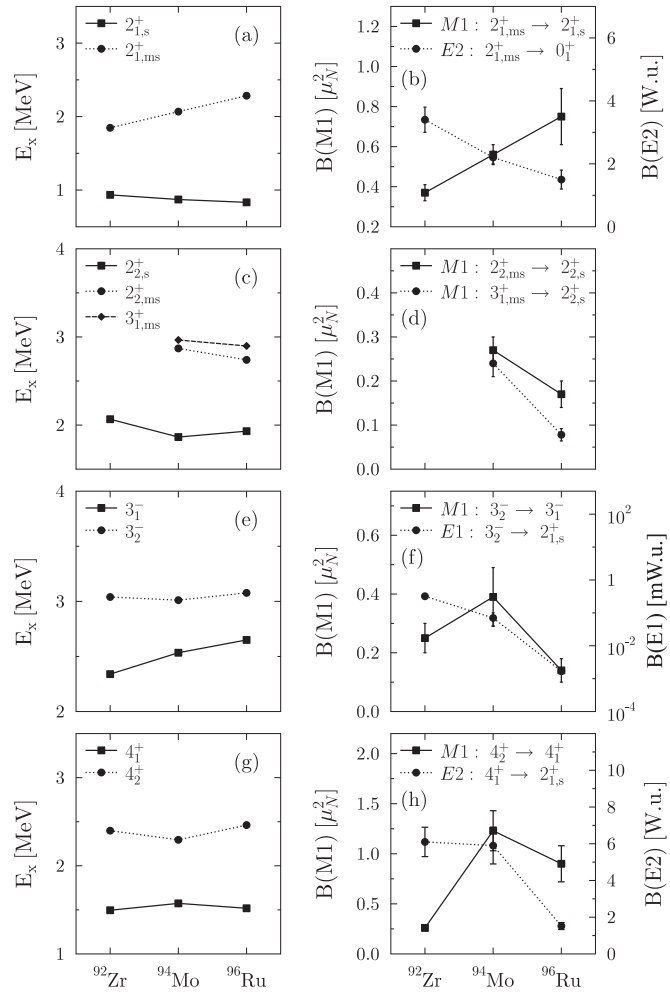

FIG. 12. Compilation of experimental data on one- and two-phonon mixed-symmetry states of the $N = 52$ isotones ^{92}Zr, ^{94}Mo, and ^{96}Ru. The left panel shows the excitation energies while the $M1$, $E1$, and $E2$ transition strengths are compiled in the right panel. Included are data on one-phonon quadrupole ($2^+_{1,\text{ms}}$) and two-phonon quadrupole ($2^+_{2,\text{ms}}$, $3^+_{1,\text{ms}}$) mixed-symmetry states in the first and second rows as well as data on candidates for one-phonon octupole (3^-_2) and hexadecapole mixed-symmetry states (4^+_2) in rows three and four. Data for ^{92}Zr and ^{94}Mo are taken from Refs. [14,15].

for the 2_2^+ state [73]. The breaking of F-spin symmetry caused by this unbalanced proton-neutron content in the wave function is referred to as configurational isospin polarization (CIP) [60,73,74]. However, the 2_2^+ state of ^{92}Zr evolves into the collective mixed-symmetry states of ^{94}Mo and ^{96}Ru to which they are compared in this discussion. Therefore, the term "mixed-symmetry state" is used for the 2_2^+ state of ^{92}Zr in the following, despite the presence of pronounced noncollective components. The first two rows of Fig. 12 show a compilation of experimental data on the excitation energies (left) and $M1$, $E1$, and $E2$ transition strengths for the symmetric (s) and mixed-symmetric (ms) one- and two-phonon quadrupole states (right) for the nuclei ^{92}Zr [15], ^{94}Mo [14], and ^{96}Ru (this work). The corresponding values for the symmetric and mixed-symmetry one-phonon octupole and hexadecapole

candidates are included in rows 3 and 4, respectively. As expected for collective excitations, their excitation energies exhibit a smooth variation as a function of proton number.

For the one-phonon quadrupole excitations (top row), an increase of the $M1$ strength is obtained for the $2^+_{1,\mathrm{ms}} \rightarrow 2^+_{1,\mathrm{s}}$ transition towards the middle of the proton $g_{9/2}$ subshell. This is in contrast to the deexcitation of the 2^+ and 3^+ members of the mixed-symmetry two-phonon quintuplet to their symmetric counterparts, where the corresponding $M1$ transition strengths decrease from ^{94}Mo to ^{96}Ru by factors of about 2 and 3, respectively. This decrease of $M1$ strengths also holds for the candidates for the one-phonon octupole and hexadecapole states for which a maximum of the $M1$ strength is obtained for ^{94}Mo. While the $B(M1)$ values for ^{94}Mo and ^{96}Ru are still comparable for the 4^+ states, they decrease by a factor of 3 in the octupole sector. Also interesting to note is the evolution of the $3^-_2 \rightarrow 2^+_1$ $E1$ transition strength, which is predicted to be strong for a mixed-symmetry one-phonon octupole character of the 3^-_2 state in the $U_{\pi\nu}(1) \otimes U_{\pi\nu}(5) \otimes U_{\pi\nu}(7)$ limit of the sdf-IBM-2. In the $N = 52$ isotones, the corresponding $E1$ strength decreases by more than two orders of magnitude from ^{92}Zr to ^{96}Ru.

VIII. SUMMARY AND CONCLUSIONS

We studied collective low-spin excitations of ^{96}Ru by means of two inelastic proton-scattering experiments. Absolute $M1$, $E1$, and $E2$ transition strengths were deduced from the combined experimental data of two experiments, which allowed for a firm identification of the 2^+ and 3^+ members of the two-phonon mixed-symmetry quintuplet as well as candidates for one-phonon mixed-symmetry octupole and hexadecapole states. The origin of the strong $4^+_2 \rightarrow 4^+_1$ $M1$ transition was investigated in the scope of shell-model calculations that were performed with a realistic interaction. From the calculations, the pn symmetry of the wave functions of low-lying 2^+ and 4^+ states was extracted. The results indicate dominant pn-symmetric and mixed-symmetric configurations for the 4^+_1 and 4^+_2 states, supporting their symmetric and mixed-symmetry one-phonon hexadecapole interpretation. These findings are in line with the results obtained from sdg-IBM-2 calculations. For a firm identification of hexadecapole contributions, a measurement of $E4$ transition strengths in ^{96}Ru is highly desirable. Experimentally, they are accessible, e.g., via inelastic electron and hadron scattering at higher energies; see, e.g., Ref. [75].

ACKNOWLEDGMENTS

The authors thank R. Casperson and S. Heinze for support with the IBM calculations as well as R.V. Jolos, A. Poves, and R. Schwengner for stimulating discussions. Furthermore, we gratefully acknowledge the support of the accelerator staff at WNSL, Yale and IKP, Cologne during the beam times, as well as H.W. Becker and D. Rogalla from the Ruhr-Universität Bochum for the assistance during the RBS measurement. This work is supported by the DFG under Grant No. ZI 510/4-2, ZI 510/7-1, and SFB 634, the U.S. Department of Energy Grant No. DE-FG02-01ER40609, and the BMBF Grant No. 05P12RDFN8. D.R. and D.S. acknowledge the German Academic Exchange Service (DAAD) for financial support. S.G.P. and M.S. are supported by the Bonn-Cologne Graduate School of Physics and Astronomy (BCGS).

[1] A. Faessler, Nucl. Phys. **85**, 653 (1966).
[2] F. Iachello, Phys. Rev. Lett. **53**, 1427 (1984).
[3] K. Heyde and J. Sau, Phys. Rev. C **33**, 1050 (1986).
[4] A. Arima and F. Iachello, Phys. Rev. Lett. **35**, 1069 (1975).
[5] A. Arima, T. Otsuka, F. Iachello, and I. Talmi, Phys. Lett. B **66**, 205 (1977).
[6] T. Otsuka, A. Arima, and F. Iachello, Nucl. Phys. A **309**, 1 (1978).
[7] P. van Isacker, K. Heyde, J. Jolie, and A. Sevrin, Ann. Phys. (N.Y.) **171**, 253 (1986).
[8] A. F. Lisetskiy, N. Pietralla, C. Fransen, R. V. Jolos, and P. von Brentano, Nucl. Phys. A **677**, 100 (2000).
[9] N. Lo Iudice and C. Stoyanov, Phys. Rev. C **62**, 047302 (2000).
[10] N. Pietralla, P. von Brentano, and A. F. Lisetskiy, Prog. Part. Nucl. Phys. **60**, 225 (2008).
[11] N. Pietralla, C. Fransen, D. Belic, P. von Brentano, C. Frießner, U. Kneissl, A. Linnemann, A. Nord, H. H. Pitz, T. Otsuka, I. Schneider, V. Werner, and I. Wiedenhöver, Phys. Rev. Lett. **83**, 1303 (1999).
[12] N. Pietralla, C. Fransen, P. von Brentano, A. Dewald, A. Fitzler, C. Frießner, and J. Gableske, Phys. Rev. Lett. **84**, 3775 (2000).
[13] C. Fransen, N. Pietralla, P. von Brentano, A. Dewald, J. Gableske, A. Gade, A. F. Lisetskiy, and V. Werner, Phys. Lett. B **508**, 219 (2001).
[14] C. Fransen, N. Pietralla, Z. Ammar, D. Bandyopadhyay, N. Boukharouba, P. von Brentano, A. Dewald, J. Gableske, A. Gade, J. Jolie, U. Kneissl, S. R. Lesher, A. F. Lisetskiy, M. T. McEllistrem, M. Merrick, H. H. Pitz, N. Warr, V. Werner, and S. W. Yates, Phys. Rev. C **67**, 024307 (2003).
[15] C. Fransen, V. Werner, D. Bandyopadhyay, N. Boukharouba, S. R. Lesher, M. T. McEllistrem, J. Jolie, N. Pietralla, P. von Brentano, and S. W. Yates, Phys. Rev. C **71**, 054304 (2005).
[16] V. Werner, D. Belic, P. von Brentano, C. Fransen, A. Gade, H. von Garrel, J. Jolie, U. Kneissl, C. Kohstall, A. Linnemann, A. F. Lisetskiy, N. Pietralla, H. H. Pitz, M. Scheck, K.-H. Speidel, F. Stedile, and S. W. Yates, Phys. Lett. B **550**, 140 (2002).
[17] J. N. Orce, J. D. Holt, A. Linnemann, C. J. McKay, S. R. Lesher, C. Fransen, J. W. Holt, A. Kumar, N. Warr, V. Werner, J. Jolie, T. T. S. Kuo, M. T. McEllistrem, N. Pietralla, and S. W. Yates, Phys. Rev. Lett. **97**, 062504 (2006).
[18] N. Pietralla, C. J. Barton, R. Krücken, C. W. Beausang, M. A. Caprio, R. F. Casten, J. R. Cooper, A. A. Hecht, H. Newman, J. R. Novak, and N. V. Zamfir, Phys. Rev. C **64**, 031301(R) (2001).
[19] H. Klein, A. F. Lisetskiy, N. Pietralla, C. Fransen, A. Gade, and P. von Brentano, Phys. Rev. C **65**, 044315 (2002).
[20] A. Linnemann, C. Fransen, M. Gorska, J. Jolie, U. Kneissl, P. Knoch, D. Mücher, H. H. Pitz, M. Scheck, C. Scholl, and P. von Brentano, Phys. Rev. C **72**, 064323 (2005).

[21] K. Heyde, P. von Neumann-Cosel, and A. Richter, Rev. Mod. Phys. **82**, 2365 (2010).
[22] G. Siems, U. Neuneyer, I. Wiedenhöver, S. Albers, M. Eschenauer, R. Wirowski, A. Gelberg, P. von Brentano, and T. Otsuka, Phys. Lett. B **320**, 1 (1994).
[23] T. Otsuka and K.-H. Kim, Phys. Rev. C **50**, R1768 (1994).
[24] N. Pietralla, P. von Brentano, R. F. Casten, T. Otsuka, and N. V. Zamfir, Phys. Rev. Lett. **73**, 2962 (1994).
[25] M. Scheck, P. A. Butler, C. Fransen, V. Werner, and S. W. Yates, Phys. Rev. C **81**, 064305 (2010).
[26] R. J. Casperson, V. Werner, and S. Heinze, Phys. Lett. B **721**, 51 (2013).
[27] N. A. Smirnova, N. Pietralla, T. Mizusaki, and P. van Isacker, Nucl. Phys. A **678**, 235 (2000).
[28] N. Pietralla, C. Fransen, A. Gade, N. A. Smirnova, P. von Brentano, V. Werner, and S. W. Yates, Phys. Rev. C **68**, 031305(R) (2003).
[29] A. Hennig, M. Spieker, V. Werner, T. Ahn, V. Anagnostatou, N. Cooper, V. Derya, M. Elvers, J. Endres, P. Goddard, A. Heinz, R. O. Hughes, G. Ilie, M. N. Mineva, P. Petkov, S. G. Pickstone, N. Pietralla, D. Radeck, T. J. Ross, D. Savran, and A. Zilges, Phys. Rev. C **90**, 051302(R) (2014).
[30] C. W. Beausang, C. J. Barton, M. A. Caprio, R. F. Casten, J. R. Cooper, R. Krücken, B. Liu, J. R. Novak, Z. Wang, M. Wilhelm, A. N. Wilson, N. V. Zamfir, and A. Zilges, Nucl. Instrum. Methods Phys. Res., Sect. A **452**, 431 (2000).
[31] M. Elvers, S. Pascu, T. Ahmed, T. Ahn, V. Anagnostatou, N. Cooper, C. Deng, J. Endres, P. Goddard, A. Heinz, G. Ilie, E. Jiang, C. Küppersbusch, D. Radeck, D. Savran, N. Shenkov, V. Werner, and A. Zilges, Phys. Rev. C **84**, 054323 (2011).
[32] K. S. Krane, R. M. Steffen, and R. M. Wheeler, At. Data Nucl. Data Tables **11**, 351 (1973).
[33] P. J. Nolan and J. F. Sharpey-Schafer, Rep. Prog. Phys. **42**, 1 (1979).
[34] T. K. Alexander and J. S. Forster, Adv. Nucl. Phys. **10**, 197 (1978).
[35] S. G. Pickstone, V. Derya, A. Hennig, J. Mayer, M. Spieker, M. Weinert, J. Wilhelmy, and A. Zilges, EPJ Web Conf. **93**, 01053 (2015).
[36] B. Hubbard-Nelson, M. Momayezi, and W. K. Warburton, Nucl. Instrum. Methods Phys. Res., Sect. A **422**, 411 (1999).
[37] G. A. P. Engelbertink and G. van Middelkoop, Nucl. Phys. A **138**, 588 (1969).
[38] G. G. Seaman, N. Benczer-Koller, M. C. Bertin, and J. R. MacDonald, Phys. Rev. **188**, 1706 (1969).
[39] A. Hennig, V. Derya, M. N. Mineva, P. Petkov, S. G. Pickstone, M. Spieker, and A. Zilges, Nucl. Instrum. Methods Phys. Res., Sect. A **794**, 171 (2015).
[40] P. Petkov, J. Gableske, O. Vogel, A. Dewald, P. von Brentano, R. Krücken, R. Peusquens, N. Nicolay, A. Gizon, J. Gizon, D. Bazzacco, C. Rossi-Alvarez, S. Lunardi, P. Pavan, D. R. Napoli, W. Andrejtscheff, and R. V. Jolos, Nucl. Phys. A **640**, 293 (1998).
[41] G. Winter, Nucl. Instrum. Methods **214**, 537 (1983).
[42] G. Winter, ZfK Rossendorf Report No. **ZfK-497**, 1983 (unpublished).
[43] L. C. Northcliffe and R. F. Schilling, At. Data Nucl. Data Tables **7**, 233 (1970).
[44] J. F. Ziegler and W. K. Chu, At. Data Nucl. Data Tables **13**, 463 (1974).
[45] J. F. Ziegler and J. P. Biersack, *Treatise on Heavy-Ion Science*, Vol. 6, edited by D. A. Bromley (Plenum Press, New York, 1985), p. 95.
[46] J. Lindhard, M. Scharff, and H. E. Schiøtt, Mat. Fys. Medd., Dan. Vid. Selsk. **33**, 1 (1963).
[47] W. M. Currie, Nucl. Instrum. Methods **73**, 173 (1969).
[48] J. Lange, J. Neuber, P. Tendler, C. D. Uhlhorn, A. T. Kandil, and H. V. Buttlar, Nucl. Phys. A **330**, 29 (1979).
[49] E. Adamides, J. Sinatkas, L. D. Skouras, A. C. Xenoulis, E. N. Gazis, C. T. Papadopoulos, and R. Vlastou, Phys. Rev. C **34**, 791 (1986).
[50] D. Abriola and A. Sonzogni, Nucl. Data Sheets **109**, 2501 (2008).
[51] S. Landsberger, R. Lecomte, P. Paradis, and S. Monaro, Phys. Rev. C **21**, 588 (1980).
[52] P. O. Lipas, Nucl. Phys. **82**, 91 (1966).
[53] P. Vogel and L. Kocbach, Nucl. Phys. A **176**, 33 (1971).
[54] M. Wilhelm, S. Kasemann, G. Pascovici, E. Radermacher, P. von Brentano, and A. Zilges, Phys. Rev. C **57**, 577 (1998).
[55] U. Kneissl, H. H. Pitz, and A. Zilges, Prog. Part. Nucl. Phys. **37**, 349 (1996).
[56] N. Pietralla, Phys. Rev. C **59**, 2941 (1999).
[57] W. Andrejtscheff, C. Kohstall, P. von Brentano, C. Fransen, U. Kneissl, N. Pietralla, and H. H. Pitz, Phys. Lett. B **506**, 239 (2001).
[58] M. Babilon, T. Hartmann, P. Mohr, K. Vogt, S. Volz, and A. Zilges, Phys. Rev. C **65**, 037303 (2002).
[59] N. Pietralla, P. von Brentano, A. Gelberg, T. Otsuka, A. Richter, N. A. Smirnova, and I. Wiedenhöver, Phys. Rev. C **58**, 191 (1998).
[60] J. D. Holt, N. Pietralla, J. W. Holt, T. T. S. Kuo, and G. Rainovski, Phys. Rev. C **76**, 034325 (2007).
[61] N. Boelaert, N. Smirnova, K. Heyde, and J. Jolie, Phys. Rev. C **75**, 014316 (2007).
[62] K. Sieja, G. Martínez-Pinedo, L. Coquard, and N. Pietralla, Phys. Rev. C **80**, 054311 (2009).
[63] C. Plettner, L. Batist, J. Döring, A. Blazhev, H. Grawe, V. Belleguic, C. R. Bingham, R. Borcea, M. Gierlik, M. Górska, N. Harrington, Z. Janas, M. Karny, R. Kirchner, C. Mazzocchi, P. Munro, E. Roeckl, K. Schmidt, and R. Schwengner, Phys. Rev. C **66**, 044319 (2002).
[64] B. A. Brown and W. D. M. Rae, Nushell@MSU, MSU-NSCL report, 2007 (unpublished).
[65] H. Grawe and M. Lewitowicz, Nucl. Phys. A **693**, 116 (2001).
[66] M. Hjorth-Jensen, T. T. S. Kuo, and E. Osnes, Phys. Rep. **261**, 125 (1995).
[67] A. Blazhev (private communication).
[68] D. Radeck, M. Albers, C. Bernards, L. Bettermann, A. Blazhev, C. Fransen, S. Heinze, J. Jolie, and D. Mücher, Nucl. Phys. A **821**, 1 (2009).
[69] D. Radeck, A. Blazhev, M. Albers, C. Bernards, A. Dewald, C. Fransen, M. Heidemann, J. Jolie, B. Melon, D. Mücher, T. Pissulla, W. Rother, K. O. Zell, and O. Möller, Phys. Rev. C **80**, 044331 (2009).
[70] R. Nikolaeva, Ch. Stoyanov, and A. I. Vdovin, Eur. Phys. Lett. **8**, 117 (1989).
[71] N. Lo Iudice and Ch. Stoyanov, Phys. Rev. C **69**, 044312 (2004).
[72] N. Lo Iudice, V. Yu. Ponomarev, C. Stoyanov, A. V. Sushkov, and V. V. Voronov, J. Phys. G **39**, 043101 (2012).
[73] V. Werner, N. Benczer-Koller, G. Kumbartzki, J. D. Holt, P. Boutachkov, E. Stefanova, M. Perry, N. Pietralla, H. Ai, K.

Aleksandrova, G. Anderson, R. B. Cakirli, R. J. Casperson, R. F. Casten, M. Chamberlain, C. Copos, B. Darakchieva, S. Eckel, M. Evtimova, C. R. Fitzpatrick, A. B. Garnsworthy, G. Gürdal, A. Heinz, D. Kovacheva, C. Lambie-Hanson, X. Liang, P. Manchev, E. A. McCutchan, D. A. Meyer, J. Qian, A. Schmidt, N. J. Thompson, E. Williams, and R. Winkler, Phys. Rev. C **78**, 031301(R) (2008).

[74] A. P. Severyukhin, N. N. Arsenyev, N. Pietralla, and V. Werner, Phys. Rev. C **90**, 011306 (2014).

[75] M. Pignanelli, N. Blasi, S. Micheletti, R. D. Leo, L. LaGamba, R. Perrino, J. A. Bordewijk, M. A. Hofstee, J. M. Schippers, S. van der Werf, J. Wesseling, and M. N. Harakeh, Nucl. Phys. A **540**, 27 (1992).